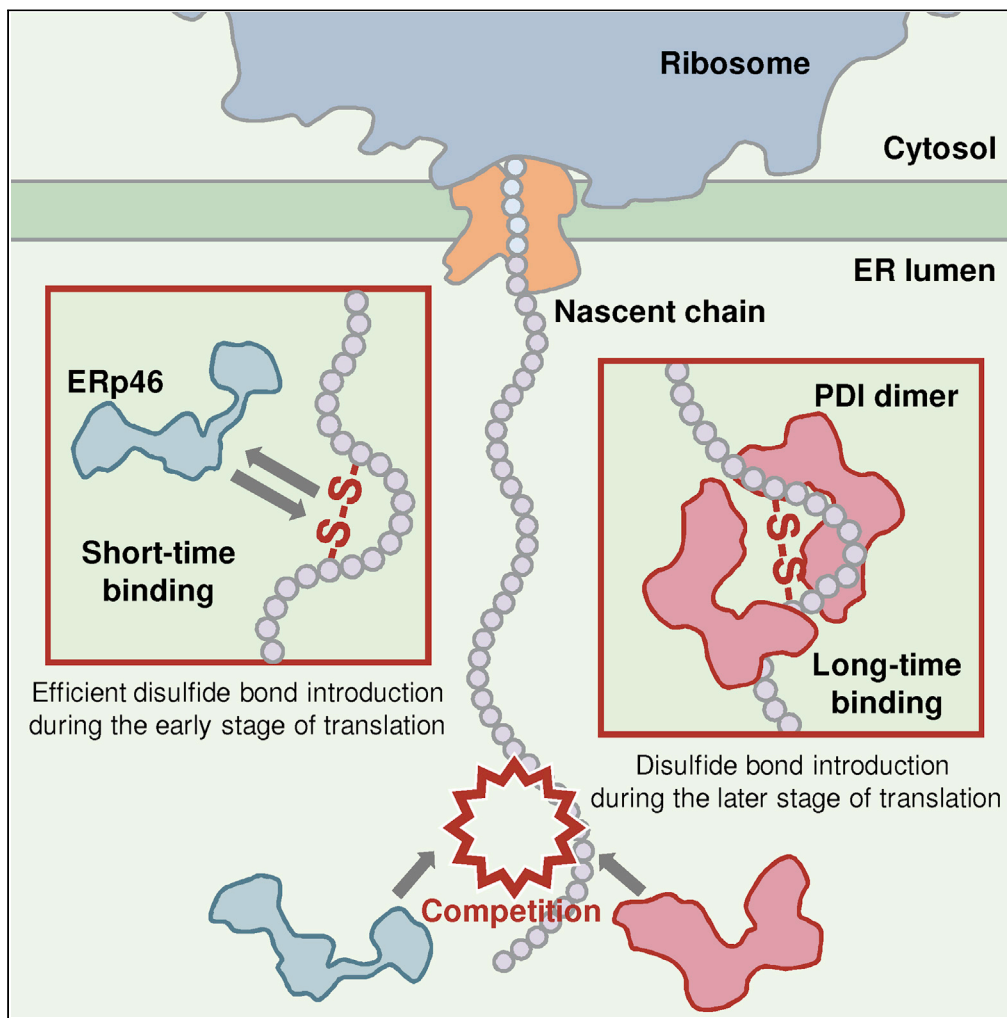


Article

Distinct roles and actions of protein disulfide isomerase family enzymes in catalysis of nascent-chain disulfide bond formation



Chihiro Hirayama,
Kodai Machida,
Kentaro Noi, ...,
Teru Ogura,
Hiroaki Imataka,
Kenji Inaba

kenji.inaba.a1@tohoku.ac.jp

Highlights

We developed an *in vitro* system for monitoring nascent-chain disulfide formation

High-speed AFM visualized PDI and ERp46 molecules acting on nascent chains

PDI persistently holds nascent chains via dimerization for disulfide introduction

ERp46 rapidly introduces disulfide bonds to nascent chains via short-time binding

Hirayama et al., iScience 24,
102296
April 23, 2021 © 2021 The
Author(s).
[https://doi.org/10.1016/
j.isci.2021.102296](https://doi.org/10.1016/j.isci.2021.102296)

Article

Distinct roles and actions of protein disulfide isomerase family enzymes in catalysis of nascent-chain disulfide bond formation

Chihiro Hirayama,¹ Kodai Machida,^{2,8} Kentaro Noi,^{3,8} Tadayoshi Murakawa,⁴ Masaki Okumura,^{1,5} Teru Ogura,^{6,7} Hiroaki Imataka,² and Kenji Inaba^{1,9,*}

SUMMARY

The mammalian endoplasmic reticulum (ER) harbors more than 20 members of the protein disulfide isomerase (PDI) family that act to maintain proteostasis. Herein, we developed an *in vitro* system for directly monitoring PDI- or ERp46-catalyzed disulfide bond formation in ribosome-associated nascent chains of human serum albumin. The results indicated that ERp46 more efficiently introduced disulfide bonds into nascent chains with a short segment exposed outside the ribosome exit site than PDI. Single-molecule analysis by high-speed atomic force microscopy further revealed that PDI binds nascent chains persistently, forming a stable face-to-face homodimer, whereas ERp46 binds for a shorter time in monomeric form, indicating their different mechanisms for substrate recognition and disulfide bond introduction. Thus, ERp46 serves as a more potent disulfide introducer especially during the early stages of translation, whereas PDI can catalyze disulfide formation when longer nascent chains emerge out from ribosome.

INTRODUCTION

Over billions of years of evolution living organisms have developed ingenious mechanisms to promote protein folding (Hartl et al., 2011). The oxidative network catalyzing protein disulfide bond formation in the endoplasmic reticulum (ER) is a prime example. Although canonical protein disulfide isomerase (PDI) and ER oxidoreductin-1 (Ero1) were previously postulated to constitute a primary disulfide bond formation pathway (Araki and Inaba, 2012; Mezghrani et al., 2001; Tavender and Bulleid, 2010), more than 20 different PDI family enzymes and multiple PDI oxidases besides Ero1 have recently been identified in the mammalian ER, suggesting the development of highly diverse oxidative networks in higher eukaryotes (Nguyen et al., 2011; Schulman et al., 2010; Tavender et al., 2010). Each PDI family enzyme is likely to play a distinct role in catalyzing the oxidative folding of different substrates, concomitant with some functional redundancy, leading to the efficient production of a wide variety of secretory proteins with multiple disulfide bonds (Bulleid and Ellgaard, 2011; Okumura et al., 2015; Sato and Inaba, 2012).

Our previous *in vitro* studies using model substrates such as reduced and denatured bovine pancreatic trypsin inhibitor (BPTI) and ribonuclease A (RNase A) demonstrated that different PDI family enzymes participate in different stages of oxidative protein folding, resulting in the accelerated folding of native enzymes (Kojima et al., 2014; Sato et al., 2013). Multiple PDI family enzymes cooperate to synergistically increase the speed and fidelity of disulfide bond formation in substrate proteins. However, whether mechanistic insights gained by *in vitro* experiments using full-length substrates are applicable to real events of oxidative folding in the ER remains an important question. Indeed, some previous works demonstrated that newly synthesized polypeptide chains undergo disulfide bond formation and isomerization co-translationally, presumably via catalysis by specific PDI family members (Kadokura et al., 2020; Molinari and Helenius, 1999; Robinson and Bulleid, 2020; Robinson et al., 2017, 2020). Furthermore, nascent chains play important roles in their own quality control by modulating the translation speed to increase the yield of native folding; if a nascent chain fails to fold or complete translation, then the resultant aberrant ribosome-nascent chain complexes (RNCs) are degraded or destabilized (Buhr et al., 2016; Chadani et al., 2017; Matsuo et al., 2017). These observations suggest that understanding real events of oxidative protein folding in cells requires systematic analysis of how PDI family enzymes act on nascent polypeptide chains during synthesis by ribosomes.

¹Institute of Multidisciplinary Research for Advanced Materials, Katahira 2-1-1, Aoba-ku, Tohoku University, Sendai, Miyagi 980-8577, Japan

²Graduate School of Engineering, University of Hyogo, Himeji, Hyogo 671-2280, Japan

³Institute for NanoScience Design, Osaka University, Toyonaka, Osaka 560-8531, Japan

⁴Graduate School of Life Science and Technology, Tokyo Institute of Technology, Yokohama, Kanagawa, 226-8503, Japan

⁵Frontier Research Institute for Interdisciplinary Sciences, Tohoku University, Sendai, Miyagi 980-8578, Japan

⁶Institute of Molecular Embryology and Genetics, Kumamoto University, Kumamoto, Kumamoto 860-0811, Japan

⁷Faculty of Life Sciences, Kumamoto University, Kumamoto, Kumamoto 862-0973, Japan

⁸These authors contributed equally

⁹Lead contact

*Correspondence: kenji.inaba.a1@tohoku.ac.jp
<https://doi.org/10.1016/j.isci.2021.102296>



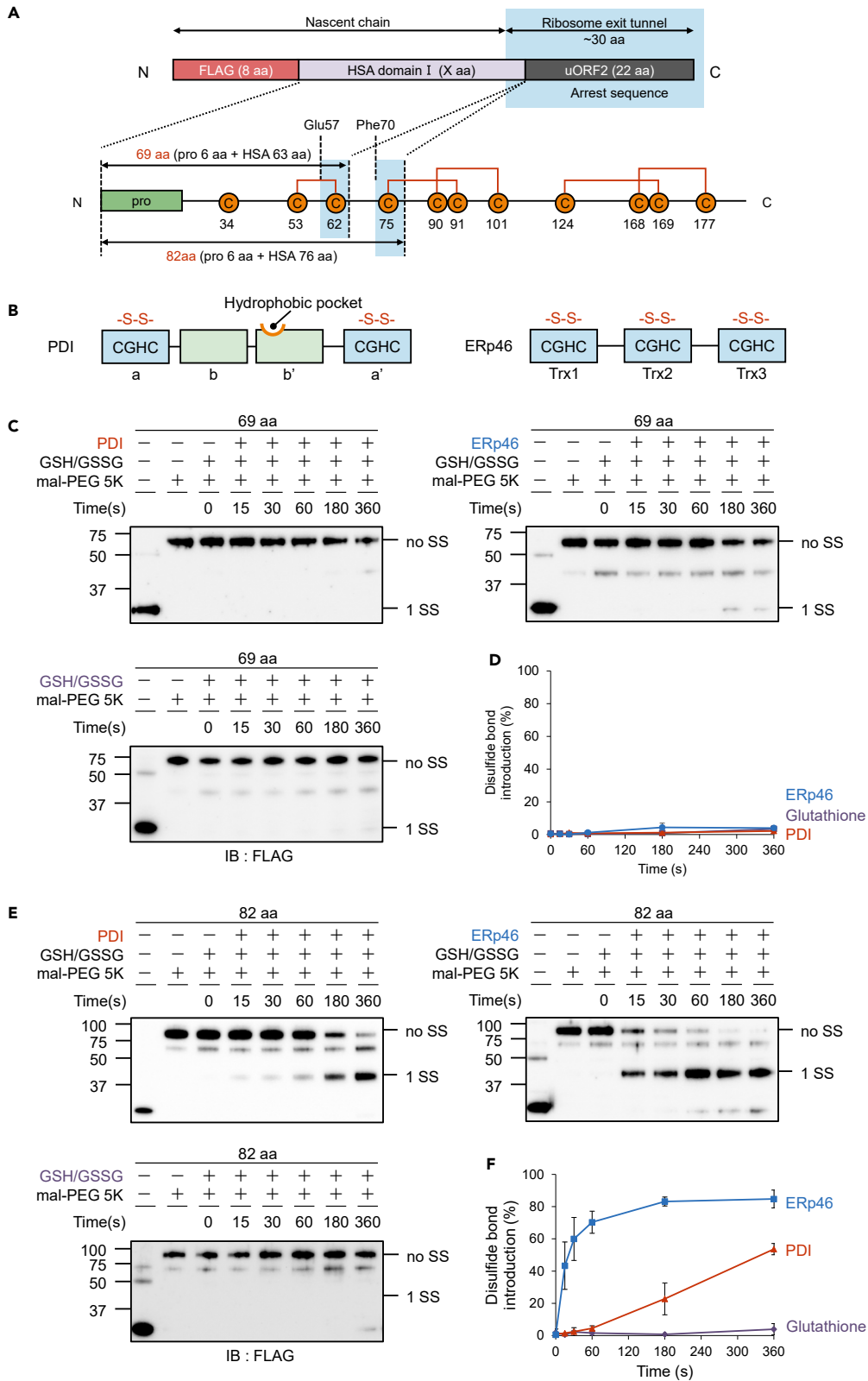


Figure 1. Disulfide bond introduction into RNC 69-aa and 82-aa by PDI and Erp46

(A) Schematic structure of plasmids constructed in this study. "uORF2" is an arrest sequence that serves to stall translation of the upstream protein and thereby prepare stable ribosome-nascent chain complexes (RNCs). The bottom cartoon represents the location of cysteines and disulfide bonds in HSA domain I. HSA domain I consists of 195 amino acids and contains five disulfide bonds and one free cysteine at residue 34. A green box indicates the pro-sequence. Orange circles and red lines indicate cysteines and native disulfide bonds, respectively. The region predicted to be buried in the ribosome exit tunnel is shown by a cyan box.

(B) Domain organization of PDI and Erp46. Redox-active Trx-like domains with a CGHC motif are indicated by cyan boxes, whereas redox-inactive ones in PDI are by light green boxes. Note that the PDI b' domain contains a substrate-binding hydrophobic pocket.

(C and E) Time course of PDI-, Erp46-, and glutathione (no enzyme)-catalyzed disulfide bond introduction into RNC 69-aa (C) and 82-aa (E). "noSS" and "1SS" denote reduced and single-disulfide-bonded species of HSA nascent chains, respectively. Note that faint bands observed between "no SS" and "1SS" likely represent a species in which one of cysteines is not subjected to mal-PEG modification due to glutathionylation. In support of this, these minor bands are even fainter under the conditions of no GSH/GSSG.

(D and F) Quantification of disulfide-bonded species for RNC 69-aa (D) and 82-aa (F) based on the results shown in (C) and (E), respectively (n = 3, mean \pm SD).

To this end, we herein developed an experimental system for directly monitoring disulfide bond formation in ribosome-associated human serum albumin (HSA) nascent chains of different lengths from the N terminus. The resultant RNCs were reacted with two ubiquitously expressed PDI family members, ER-resident protein 46 (Erp46) and canonical PDI. These two enzymes were previously shown to have distinct roles in catalyzing oxidative protein folding: Erp46 engages in rapid but promiscuous disulfide bond introduction during the early stages of folding, whereas PDI serves as an effective proofreader of non-native disulfides during the later stages (Kojima et al., 2014; Sato et al., 2013). The subsequent maleimidyl polyethylene glycol (mal-PEG) modification of free cysteines and Bis-Tris (pH7.0) PAGE (Nu-PAGE) analysis enabled us to detect the oxidation status of the HSA nascent chains conjugated with transfer RNA (tRNA). Using high-speed atomic force microscopy (HS-AFM), we further visualized PDI and Erp46 acting on the RNCs at the single-molecule level. Collectively, the results indicated that although both Erp46 and PDI could introduce a disulfide bond into the ribosome-associated HSA nascent chains, they demanded different lengths of the HSA segment exposed outside the ribosome exit site and displayed different mechanisms of action against the RNC. The present systematic *in vitro* study using RNC containing different lengths of HSA nascent chains mimics co-translational disulfide bond formation in the ER, and the results provide a framework for understanding the mechanistic basis of oxidative nascent-chain folding catalyzed by PDI family enzymes.

RESULTS

The efficiency of disulfide bond introduction into HSA nascent chains by PDI/Erp46

To investigate whether PDI family enzymes can introduce disulfide bonds into a substrate during translation, we first prepared RNCs *in vitro*. For this purpose, we made use of a cell-free protein translation system reconstituted with eukaryotic elongation factors 1 and 2, eukaryotic release factors 1 and 3 (eRF1 and eRF3), aminoacyl-tRNA synthetases, tRNAs, and ribosome subunits, developed previously by Imataka and colleagues (Machida et al., 2014). HSA was chosen as a model substrate for the following reasons. First, the three-dimensional structure of HSA has been solved at high resolution (Sugio et al., 1999), providing information on the exact location of 17 disulfide bonds in its native structure. Second, native-state HSA contains an unpaired cysteine, Cys34, near the N-terminal region, which has the potential to form a non-native disulfide bond with one of the subsequent cysteines, serving as a good indicator of whether a non-native disulfide is introduced by Erp46 or PDI during the early stage of translation. Third, the overall conformation and kinetics of disulfide bond regeneration were characterized for reduced full-length HSA (Lee and Hirose, 1992), which is beneficial for discussing similarities and differences in post- and co-translational oxidative folding. Fourth, no N-glycosylation sites are contained in the first 95 amino acids of HSA, implying that HSA nascent chains synthesized by the cell-free system are equivalent to those synthesized in the ER with regard to N-glycosylation. Finally, the involvement of PDI family enzymes in intracellular HSA folding has been demonstrated (Koritzinsky et al., 2013; Rutkevich et al., 2010; Rutkevich and Williams, 2012), ensuring the physiological relevance of the present study.

To stall the translation of HSA at specified sites, a uORF2 arrest sequence (Alderete et al., 1999) was inserted into appropriate sites of the expression plasmid (Figure 1A). We first prepared two versions of

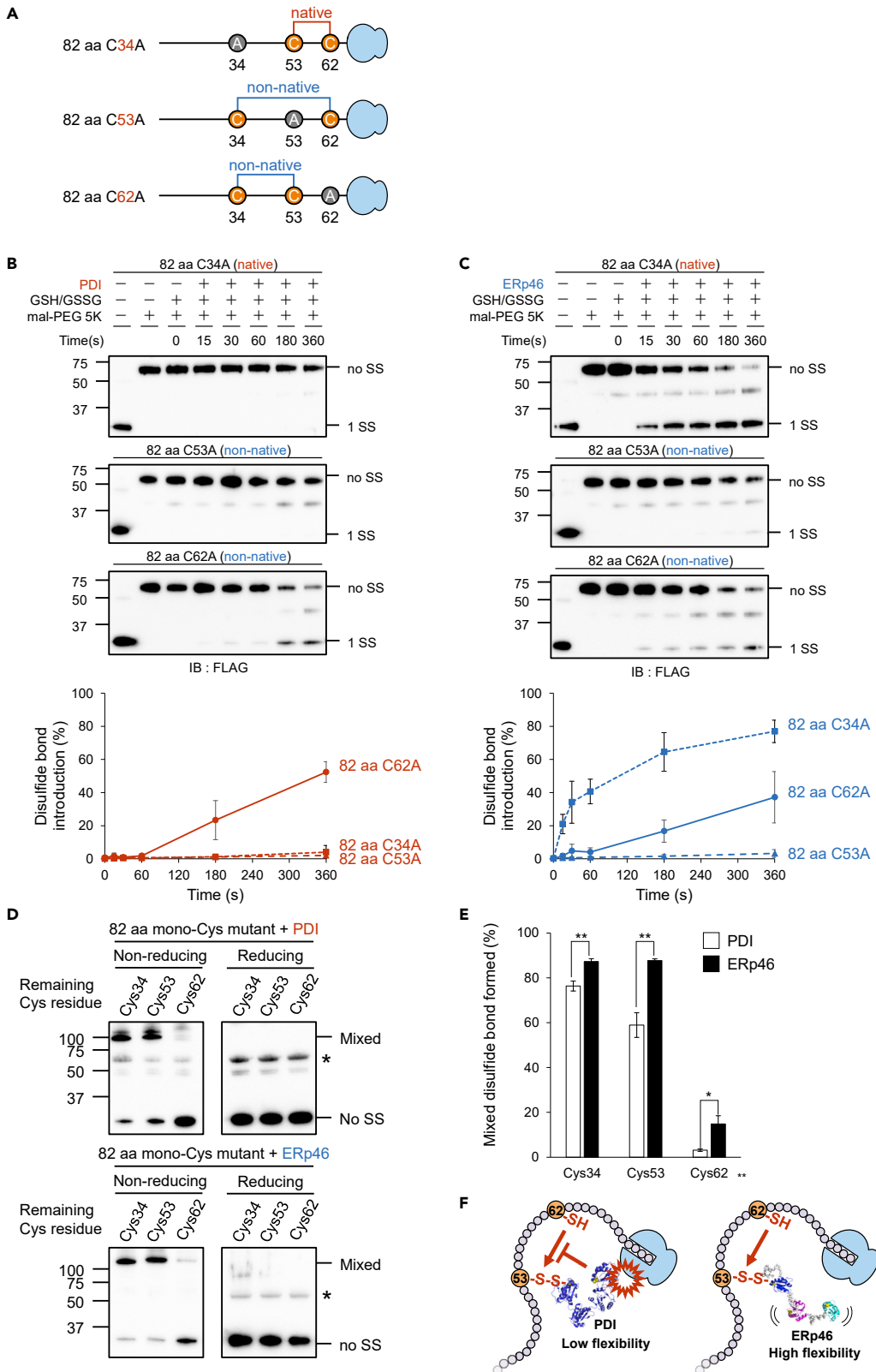


Figure 2. Disulfide bond introduction into RNC 82-aa Cys mutants by PDI and ERp46

(A) Cartoon of RNC constructs used in this study. In each construct, a cysteine (represented by a black circle) was mutated to alanine. Note that RNC 82-aa C34A retains a native cysteine pairing (i.e., Cys53 and Cys62), whereas RNC 82-aa C53A and C62A retain a non-native pairing.

(B and C) Time course of PDI- and ERp46-catalyzed disulfide bond introduction into RNC 82-aa C34A (top), C53A (middle), and C62A (bottom) mutants. Note that faint bands observed between “no SS” and “1SS” likely represent a species in which one of the cysteines is not subjected to mal-PEG modification due to glutathionylation. Quantification of disulfide-bonded species of RNC 82-aa Cys mutants is based on the results shown for the upper raw data ($n = 3$, mean \pm SD).

(D) Formation of a mixed disulfide bond between RNC 82-aa mono-Cys mutants and PDI (upper)/ERp46 (lower). “Mixed” and “No SS” denote a mixed disulfide complex between PDI/ERp46 and RNC mono-Cys mutants and isolated RNC 82-aa, respectively. Note that faint bands observed between “Mixed” and “no SS” are likely non-specific bands, as they were seen at the same position regardless of which 82-aa mono-Cys mutant was tested or whether an RNC was reacted with PDI or ERp46. (E) Quantification of mixed disulfide species based on the results shown in (D). * $p < 0.05$, ** $p < 0.01$. $n = 3$. Error bars indicate SD.

(F) The cartoon on the left shows possible steric collisions between ribosomes and PDI when Cys62 attacks the mixed disulfide between Cys53 on RNC 82-aa and PDI (left). The cartoon on the right shows that ERp46 can avoid this steric collision due to its higher flexibility and domain arrangement.

the RNC containing different lengths of HSA nascent chains: RNC 69-aa and RNC 82-aa. As the ribosome exit tunnel accommodates a polypeptide chain of ~ 30 amino acid (aa) residues (Zhang et al., 2013), the N-terminal 57 residues of HSA (excluding the N-terminal 6-aa pro-sequence) are predicted to be exposed outside the ribosome exit tunnel in RNC 69-aa, including Cys34 and Cys53 (Figure 1A). In the RNC 82-aa construct, the N-terminal 70 residues of HSA, including Cys62 and Cys34/Cys53, are predicted to emerge from the ribosome (Figure 1A). Notably, Cys53 and Cys62 form a native disulfide bond, whereas Cys34 is unpaired in the native structure of HSA domain I.

When RNC 69-aa was employed as a substrate, neither PDI nor ERp46 could efficiently introduce a disulfide bond into the nascent chain (Figures 1C and 1D). However, both enzymes introduced a disulfide bond into RNC 82-aa with higher efficiency than into RNC 69-aa (Figures 1E and 1F), suggesting that the length of the exposed HSA segment or the distance of a pair of cysteines from the ribosome exit site is critical for disulfide bond introduction by PDI and ERp46. For either construct, a faint band was seen between the bands of “no SS” and “1 SS,” and this band was even fainter without GSH/GSSG (the second lane from the left) and had a tendency to get stronger at late time points. Presumably, this band represents a species in which one of the free cysteines is glutathionylated, and the species increased gradually in the course of the reaction.

Of note, ERp46 introduced a disulfide bond into RNC 82-aa at a much higher rate than PDI, indicating that ERp46 serves as a more competent disulfide bond introducer to RNCs than PDI (Figure 1F). The remarkable difference in disulfide bond introduction efficiency by these two enzymes seems unlikely to be explained simply by the different number of redox-active Trx-like domains in PDI (two) and ERp46 (three) (Figure 1B). Also, the redox states in the presence of 1 mM GSH and 0.2 mM GSSG are similar between these two enzymes (Figures S1A and S1B), suggesting their comparable redox potentials. Thus the different ability of ERp46 and PDI to introduce a disulfide into 82-aa is likely caused by other factors such as their different structural features and different mechanisms of substrate recognition, as discussed below.

Next, to identify which cysteine pair forms a disulfide bond in RNC 82-aa, we constructed three cysteine mutants in which Cys34, Cys53, or Cys62 was mutated to alanine (Figure 2A). The assays using the mutants showed that whereas PDI was unable to introduce a disulfide bond into RNC 82-aa C34A and C53A (Figure 2B, top and middle), the enzyme introduced a Cys34-Cys53 non-native disulfide bond into RNC 82-aa C62A (Figure 2B, bottom), at almost the same rate as the generation of the “1 SS” species in 82-aa (Figures 1E and 1F). PDI could not introduce a Cys53-Cys62 native disulfide bond, presumably because this cysteine pair is located too close to the ribosome exit site (see also Figures 3B and 3C). Conversely, the slow but possible formation of a Cys34-Cys53 non-native disulfide in 82 aa by PDI suggests that the distance between a cysteine pair of interest and the ribosome exit site is key to allowing the enzyme to catalyze disulfide bond introduction into RNCs. Considering the different locations of the Cys34-Cys53 and Cys53-Cys62 pairs on RNC 82-aa, a distance of ~ 18 residues from the ribosome exit site appears to be necessary for the PDI-catalyzed reaction (see also the first paragraph of discussion).

In contrast to PDI, ERp46 could introduce a native disulfide bond into RNC 82-aa C34A (Figure 2C, top). Like PDI, ERp46 also introduced a non-native disulfide bond between Cys34 and Cys53 into RNC 82-aa C62A,

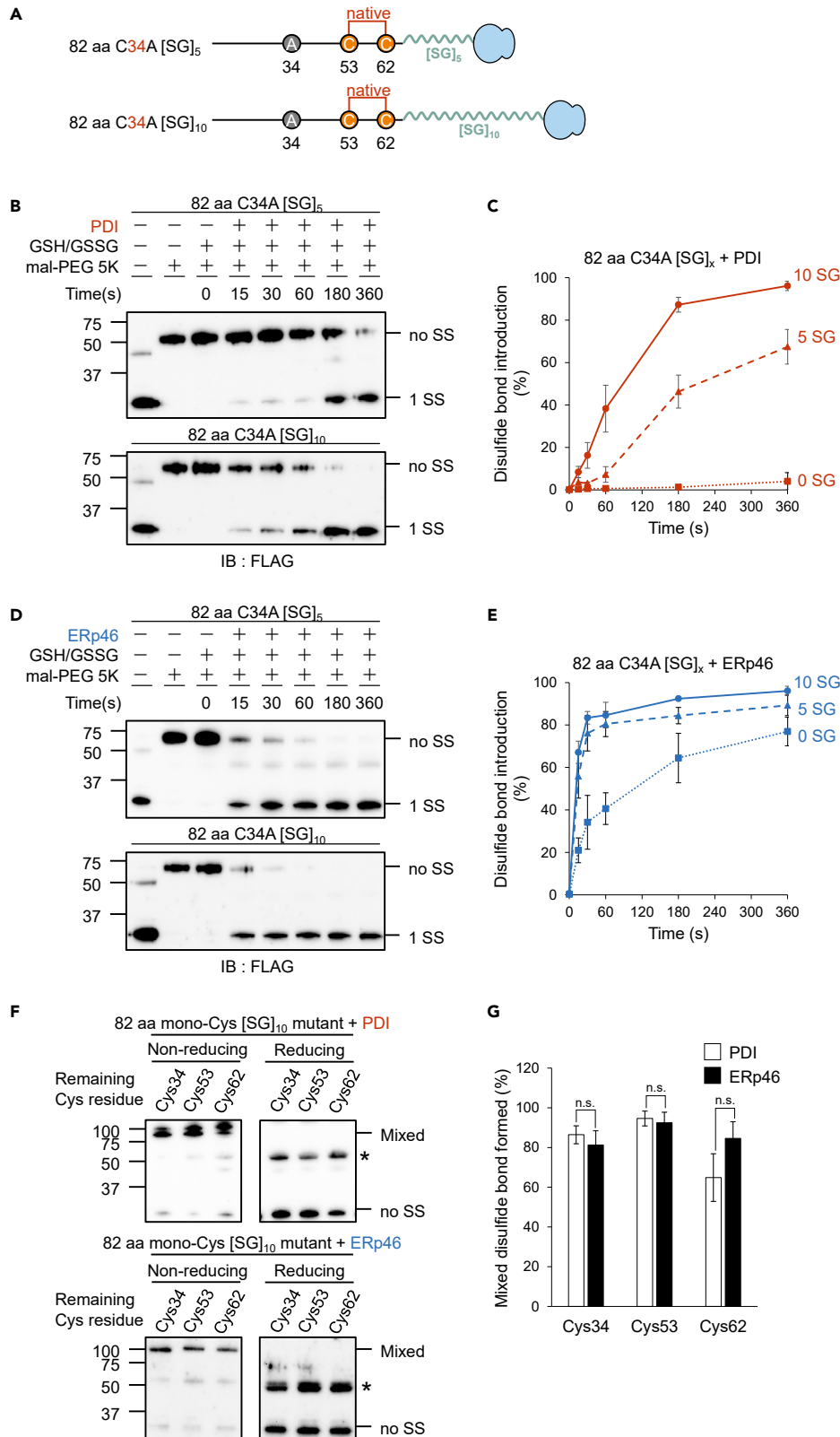


Figure 3. Correlation of the distance between Cys residues and the ribosome exit site with the efficiency of disulfide bond introduction by PDI/ERp46

(A) Cartoons of RNC constructs with [SG]-repeat insertions. An [SG]₅ or [SG]₁₀ repeat sequence was inserted into RNC-82 aa C34A immediately after Cys62.

(B and D) PDI- (B) and ERp46 (D)-mediated disulfide bond introduction into RNC 82-aa C34A with insertion of [SG]₅ (upper) or [SG]₁₀ (lower) repeats after Cys62.

(C and E) Quantification of disulfide-bonded species (1SS) based on the results shown in (B) and (D). n = 3 for PDI and 2 for ERp46. Error bars indicate SD.

(F) Formation of a mixed disulfide bond between the 82-aa mono-Cys mutant with a [SG]₁₀ repeat and PDI (upper)/ERp46 (lower). Note that bands observed between "Mixed" and "no SS" are likely non-specific bands, as they were seen at the same position regardless of which 82-aa mono-Cys [SG]₁₀ mutant was tested or whether the RNCs were reacted with PDI or ERp46.

(G) Quantification of mixed disulfide species based on the results shown in (F). n = 3. Error bars indicate SD.

but its efficiency was lower than that of a Cys53-Cys62 native disulfide (Figure 2C, bottom). No disulfide bond was formed between Cys34 and Cys62 by either ERp46 or PDI (Figure 2C, middle), presumably due to the considerable spatial separation of these two cysteines. Based on these results, we concluded that for efficient disulfide bond introduction into RNCs, ERp46 requires an intermediary polypeptide segment with a shorter distance between a cysteine pair of interest and the ribosome exit site than PDI. We here note that ERp46-catalyzed generation of the "1 SS" species was faster in 82-aa than in 82-aa C34A (Figures 1F and 2C). This observation may suggest the occurrence of Cys34-mediated disulfide bond formation in 82-aa, namely, the formation of a Cys34-Cys53 non-native disulfide and, possibly, its rapid isomerization to a Cys53-Cys62 native disulfide.

Accessibility of PDI/ERp46 to cysteines on the ribosome-HSA nascent chain complex

To examine the accessibility of PDI and ERp46 to Cys residues on RNC 82-aa, we constructed three RNC 82-aa mono-Cys mutants in which Cys34, Cys53, or Cys62 on the HSA nascent chain was retained and investigated whether a mixed disulfide could be formed between the RNC 82-aa mutant and a trapping mutant of PDI or ERp46 in which all CXXC redox-active sites were mutated to CXXA. Both PDI and ERp46 formed a mixed disulfide bond with Cys34 and Cys53 on RNC 82-aa with high probability, but covalent linkages to Cys62 were marginal (Figures 2D and 2E). The results suggest that the redox-active sites of PDI and ERp46 could gain access to Cys34 and Cys53, but to a much lesser extent, to Cys62, probably due to steric collision with the ribosome. Nevertheless, ERp46 efficiently introduced a native disulfide bond between Cys53 and Cys62 (Figure 2C, top). One possible explanation is that ERp46 first attacks Cys53 on the HSA nascent chain, and the resultant mixed disulfide is subjected to nucleophilic attack by Cys62 (Figure 2F, right). By contrast, the mixed disulfide between PDI and Cys53 on the HSA nascent chain may hardly be attacked by Cys62 due to possible steric collision between PDI and the ribosome (Figure 2F, left). In line with this idea, PDI adopts a U-like overall conformation with restricted movements of four thioredoxin (Trx)-like domains (Tian et al., 2006; Wang et al., 2012), whereas ERp46 forms a highly flexible V-shape conformation composed of three Trx-like domains and two long (~20 aa) interdomain linkers (Kojima et al., 2014).

Correlations between cysteine accessibility and the efficiency of disulfide bond introduction by PDI/ERp46

Based on the results presented above, we believe that the distance between cysteines of interest and the ribosome exit site is critical for efficient disulfide introduction by PDI and ERp46. To test this hypothesis, we increased the distance of the Cys53-Cys62 pair from the ribosome exit site by inserting an extended polypeptide segment composed of [SG]₅ or [SG]₁₀ repeat immediately after Cys62 on RNC 82-aa C34A (Figure 3A) and investigated the effects of the insertions on the efficiency of disulfide bond formation. PDI was unable to introduce a Cys53-Cys62 native disulfide into RNC 82-aa C34A (Figure 2B, top), whereas insertion of a [SG]₅ repeat allowed this reaction, and nearly 70% of 82-aa C34A was disulfide bonded within a reaction time of 360 s (Figure 3B, upper and 3C). The insertion of a longer repeat [SG]₁₀ further promoted disulfide bond formation (Figure 3B, lower and 3C).

A similar enhancement following [SG]-repeat insertion was observed for ERp46-catalyzed reactions. However, ERp46 exhibited a striking difference from PDI: insertion of a [SG]₅ repeat was long enough to introduce a Cys53-Cys62 native disulfide into RNC 82-aa C34A within 15 s, and insertion of a [SG]₁₀ repeat gave only a small additional enhancement (Figures 3D and 3E). Thus, the presence of a disordered or extended segment of ~18 aa (Asp63–Phe70 + [SG]₅ repeat) between a cysteine pair of interest and the ribosome exit

site seemed necessary and sufficient for ERp46 to generate a Cys53-Cys62 disulfide rapidly, whereas PDI required a longer segment of ~28 aa (Asp63–Phe70 + [SG]₁₀ repeat) in this intermediary region for efficient introduction of a Cys53-Cys62 disulfide. Thus ERp46 appears to be more capable of introducing a disulfide bond near the ribosome exit site than PDI. In other words, ERp46 likely has the greater potential to introduce a disulfide bond into the HSA nascent chain during the earlier stages of translation than PDI.

To verify that Cys53-Cys62 disulfide formation facilitated by [SG]₁₀ repeat insertion was ascribed to higher accessibility of PDI/ERp46 to Cys62, we again investigated mixed disulfide bond formation between trapping mutants of PDI/ERp46 and each cysteine on RNC 82-aa following [SG]₁₀ repeat insertion. Both PDI and ERp46 formed a mixed disulfide with all cysteines including Cys62 (Figures 3F and 3G), indicating that there is a correlation between the accessibility of PDI/ERp46 to a target pair of cysteines and the efficiency of disulfide bond introduction by the enzymes.

Disulfide bond introduction into a longer HSA nascent chain by PDI/ERp46

In addition to the [SG]-repeat insertion, we examined the effect of natural HSA sequence extension on PDI- or ERp46-mediated disulfide formation. For this purpose, we prepared RNC 95-aa in which the N-terminal 83 amino acids of HSA (excluding the N-terminal 6-aa pro-sequence), including Cys34, Cys53, Cys62, and Cys75, are predicted to emerge from ribosome (Figure S2A). With this construct, however, we had a technical problem with detection of the reduced species, because mal-PEG modification of four cysteines greatly diminished the gel-to-membrane transfer efficiency. We overcame this problem by using photo-cleavable mal-PEG (PEG-PCMal) and irradiating UV light to the SDS gel after the gel electrophoresis and before the membrane transfer.

Consequently, we observed that ERp46 introduced a disulfide bond into RNC 95-aa more rapidly than PDI (Figures S2B and S2C), in agreement with our conclusion that ERp46 has the greater potential to introduce a disulfide bond into the HSA nascent chain than PDI. However, the efficiency of disulfide introduction into 95-aa was lower than that into 82-aa (Figures 1E and 1F), although a longer polypeptide chain is exposed outside the ribosome exit site in RNC 95-aa. In this regard, the effect of natural sequence extension was opposite to that of [SG]-repeat insertion. Formation of some higher-order structure or exposure of another cysteine may somehow prevent PDI and ERp46 from introducing a disulfide bond into RNC 95-aa. Thus, a longer polypeptide chain exposed outside ribosome does not always lead to higher disulfide formation rates. It is suggested that PDI and ERp46 can introduce a disulfide bond into a nascent chain with higher efficiency when the necessary and minimum length emerges out.

Given that four cysteines are exposed outside ribosome in RNC 95-aa, we next investigated whether the co-presence of PDI and ERp46 can accelerate nascent-chain disulfide formation additionally or synergistically. The mixture of PDI and ERp46 generated a “1 SS” species, but not a “2 SS” species, like PDI or ERp46 alone (Figures S2B and S2C). Notably, the presence of PDI rather inhibited ERp46-mediated disulfide formation, possibly due to its competition with ERp46 for binding to RNC 95-aa. Thus, neither additional nor synergistic effect was observed for disulfide bond formation in the ribosome-associated HSA nascent chain catalyzed by the co-presence of PDI and ERp46.

Single-molecule analysis of ERp46 by high-speed atomic force microscopy

To explore the mechanisms by which PDI and ERp46 recognize and act on RNCs at the molecular level, we employed HS-AFM (Kodera et al., 2010; Noi et al., 2013; Okumura et al., 2019; Uchihashi et al., 2018). Although our previous HS-AFM analysis revealed that PDI molecules form homodimers in the presence of unfolded substrates (Okumura et al., 2019), the structure and dynamics of ERp46 have not been analyzed using this experimental approach. Therefore, we first observed ERp46 molecules alone by immobilizing the N-terminal His-tag on a Co²⁺-coated mica surface. AFM images revealed various overall shapes of ERp46 (Figure 4A), and some particle images clearly demonstrated the presence of three thioredoxin (Trx)-like domains in ERp46 (Figure 4A, left). To assess the overall structures of ERp46, we calculated the circularity of each molecule and performed statistical analysis (Uchihashi et al., 2018). Circularity is a measure of how circular the outline of an observed molecule is, defined by the equation $4\pi S/L^2$, where L and S are the contour length of the outline and the area surrounded by the outline, respectively. Thus a circularity of 1.0 indicates a perfect circle, and values < 1 indicate a more extended conformation.

Statistical analysis based on circularity classified randomly chosen ERp46 particles into two major groups: open V-shape and round/compact O-shape (Figure 4A). Histograms with Gaussian fitting curves indicated

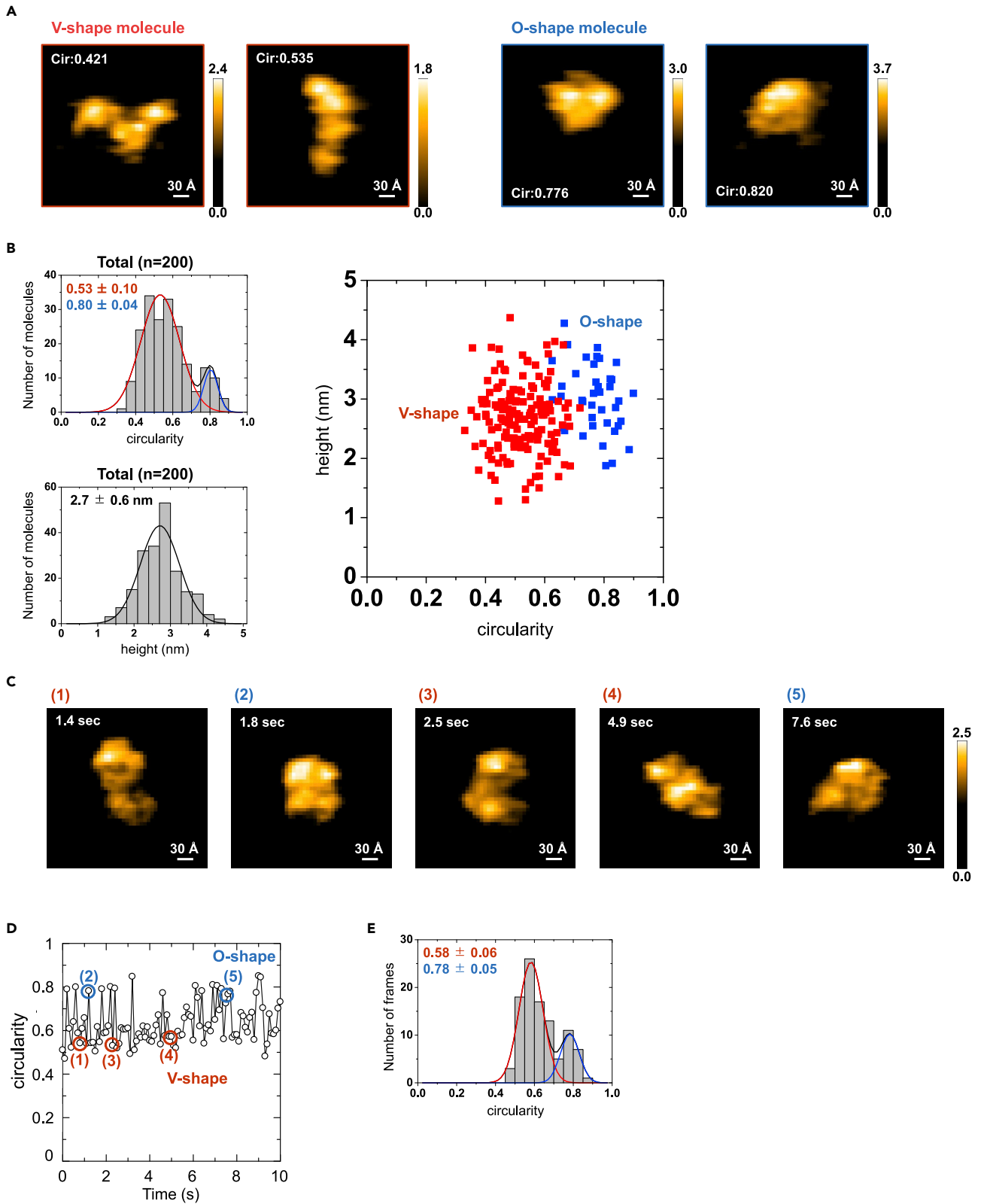


Figure 4. High-speed AFM analysis of ERp46

- (A) AFM images (scan area, 300 × 300 Å; scale bar, 30 Å) for ERp46 V-shape (left) and O-shape (right) conformations. (B) Left upper: Histograms of circularity calculated from AFM images of ERp46. Values represent the average circularity (mean ± SD) calculated from curve fitting with a single- (middle and right) or two- (left) Gaussian model. Left lower: Histograms of height calculated from AFM images of ERp46. Values represent the average height (mean ± SD) calculated from curve fitting with a single-Gaussian model. Right: Two-dimensional scatterplots of the height versus circularity for ERp46 molecules observed by HS-AFM. (C) Time course snapshots of oxidized ERp46 captured by HS-AFM. The images were traced for 10 s. See also [Video S1](#). (D) Time trace of the circularity of an ERp46 molecule. (E) Histogram of the circularity of ERp46 calculated from the time course snapshots shown in (D).

that ~80% of ERp46 molecules adopted V-shape conformations, whereas ~20% adopted O-shape conformations (Figure 4B). There was no large difference in height between these two conformations, suggesting that the three Trx-like domains of ERp46 are arranged within the same plane in either conformation. Successive AFM images acquired every 100 ms revealed that ERp46 adopted an open V-shape conformation during nearly 75% of the observation time, whereas the protein also adopted an O-shape conformation occasionally (Figures 4C–4E and [Video S1](#)). The histogram calculated from the time course snapshots was similar to that calculated from images of 200 molecules at a certain time point (Figures 4B and 4E). Importantly, structural insights gained by HS-AFM analysis are in good agreement with those from small-angle X-ray scattering analysis: both analyses consistently indicate the coexistence of a major population of molecules with an open V-shape and a minor population with a compact O-shape (Kojima et al., 2014).

Single-molecule analysis of PDI/ERp46 acting on 82-aa RNC by HS-AFM

PDI and ERp46 are predicted to bind RNCs transiently during disulfide bond introduction, but transient interactions would make it harder to observe and analyze the mode of PDI/ERp46 binding to RNCs. More practically, at least 5 min are required to initiate the HS-AFM measurements after adding PDI or ERp46 to RNCs immobilized onto a mica surface. If we employed RNCs containing natural HSA sequences, PDI or ERp46 would complete nascent-chain disulfide formation during this setup time. We therefore constructed HSA 82-aa RNC with Cys34, Cys53, and Cys62 mutated to Ala (hereafter referred to as 82-aa CA RNC), with the intension of trapping RNC molecules bound to PDI/ERp46. After testing several RNC immobilization methods, we chose to immobilize RNC on a Ni²⁺-coated mica surface. As a result, most RNC molecules were observed to lie sideways on the mica surface, whereas nascent chains were difficult to visualize, probably due to their flexible and extended structural nature (Figure 5A).

When oxidized PDI or ERp46 was added onto the RNC-immobilized mica surface, PDI/ERp46-like particles were observed in the peripheral region of ribosomes. When no-chain RNC (NC-RNC), comprising only the N-terminal FLAG tag and the subsequent uORF2 but no segment from HSA, was immobilized on the mica surface, far fewer particles were observed near RNCs (within 25 Å from the outline of ribosomes) by HS-AFM despite the presence of PDI/ERp46 (Figures S3A and S3B). These results confirm that we successfully observed PDI/ERp46 molecules acting on HSA nascent chains associated with ribosomes.

Notably, the HS-AFM analysis revealed that PDI bound RNCs in both monomeric and dimeric forms at an approximate ratio of 7:3 (Figure 5B), as reported previously for reduced and denatured BPTI and RNase A as substrates (Okumura et al., 2019). Thus, PDI likely recognizes HSA nascent chains in a similar manner to full-length substrates. Statistical analysis of RNC binding rates revealed that whereas most monomeric PDI molecules (52/55 molecules) bound RNC for 10 s or shorter (Figures 5D and S4A and [Video S2](#)), most homodimeric PDI molecules (17/19 molecules) bound RNC for 60 s or longer (Figures 5D and S4B and [Video S3](#)). By contrast, ERp46 molecules in the periphery of RNCs were only present in monomeric form (Figure 5C). Importantly, nearly 20% (12/59 molecules) of ERp46 molecules bound RNC for 10–20 s (Figures 5D and S4C and [Video S4](#)), whereas a smaller portion (8/59 molecules) bound RNC for ~60 s (Figure 5D). It is also notable that significant portion of PDI and ERp46 molecules bound ribosomes for <5 s. This may indicate that PDI/ERp46 binds or approaches RNCs only transiently possibly via diffusion, without tight interactions.

The histogram of the distance between the edge of ribosomes and the center of ribosome-neighboring PDI/ERp46 molecules indicated that both PDI and ERp46 bound RNCs at positions ~16 nm distant from ribosomes with a single-Gaussian distribution with a half-width of ~11 nm (Figure 5E), suggesting that both enzymes recognize similar sites of the HSA nascent chain. Given that the distance between adjacent amino acids is approximately 3.5 Å along an extended strand, Cys34, Cys53, and Cys62 are calculated to be

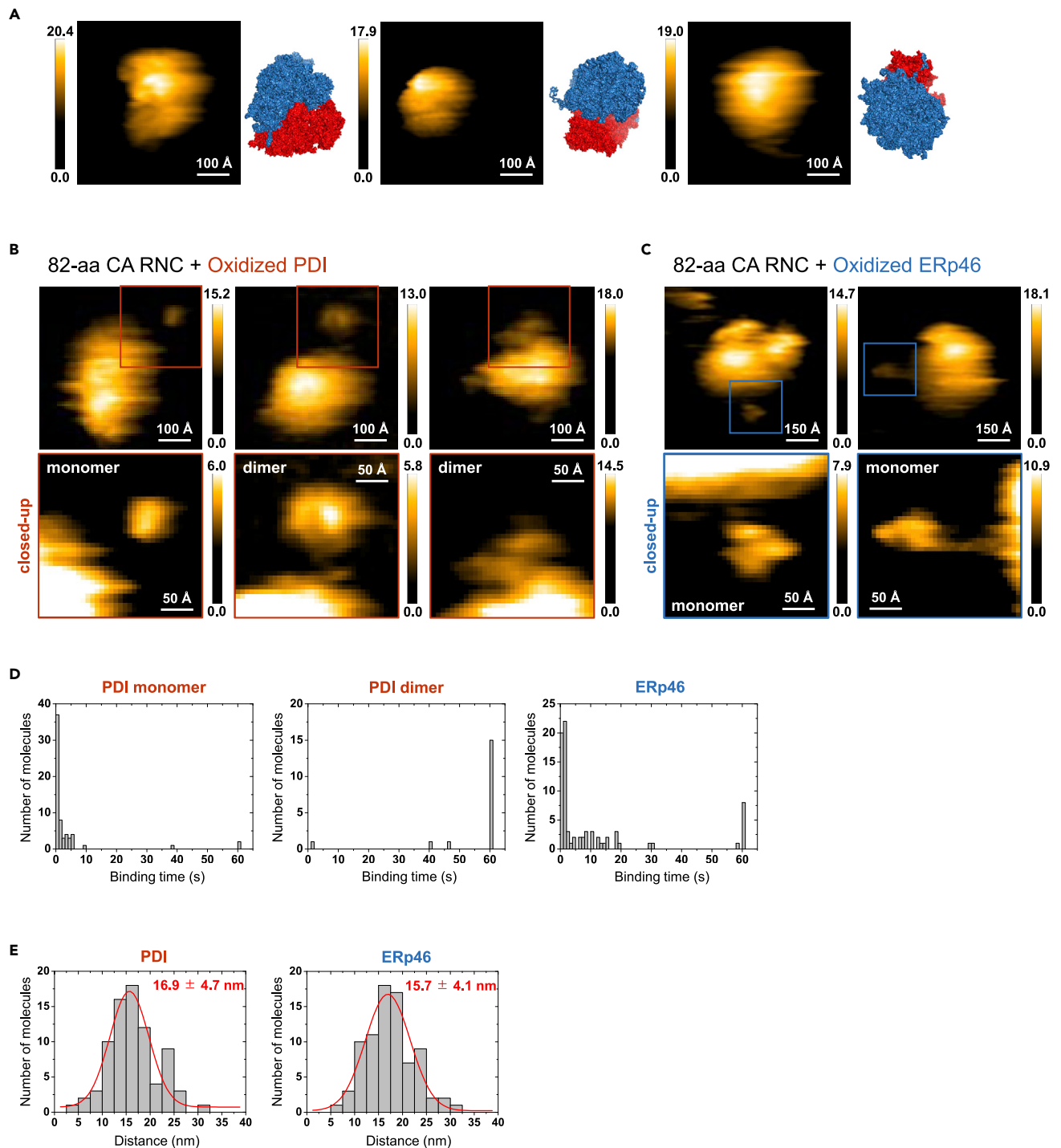


Figure 5. Single-molecule observation of PDI/Erp46 acting on 82-aa CA RNC by high-speed atomic force microscopy

(A) The AFM images (scan area, 500 Å × 500 Å; scale bar, 100 Å) displaying 82-aa CA RNC in the absence of PDI family enzymes on a Ni²⁺-coated mica surface. The surface model on the right side of each AFM image illustrates ribosome whose view angle is approximately adjusted to the observed RNC particle. 40S and 60S ribosomal subunits are shown in red and blue, respectively.

(B) Upper AFM images (scan area, 500 Å × 500 Å; scale bar, 100 Å) displaying 82-aa CA RNC in the presence of oxidized PDI (1 nM). PDI molecules that appear to bind 82-aa CA RNC are marked by red squares. Lower images (scan area, 250 Å × 250 Å; scale bar, 50 Å) highlight the regions surrounded by red squares in the upper images. See also [Videos S2](#) and [S3](#).

Figure 5. Continued

(C) Upper AFM images (scan area, 750 Å × 750 Å; scale bar, 150 Å) displaying 82-aa CA RNC in the presence of oxidized ERp46 (1 nM). ERp46 molecules that appear to bind 82-aa CA RNC are marked by blue squares. Lower images (scan area, 250 Å × 250 Å; scale bar, 50 Å) highlight the regions surrounded by blue squares in the upper images. See also [Video S4](#).

(D) Histograms of the RNC binding time of the PDI monomer (left), the PDI dimer (middle), and ERp46 (right), calculated from the observed AFM images. (E) Histograms of the distance between the edge of the ribosome and the centers of RNC-neighboring PDI (left) and ERp46 (right) molecules, calculated from the observed AFM images. Values represent the average distance (mean ± SD) calculated from curve fitting with a single-Gaussian model.

130 Å, 63 Å, and 35 Å distant from the ribosome exit site, respectively. The distributions of PDI and ERp46 molecules bound to RNC 82-aa seem consistent with their accessibility to Cys34 and Cys53, but not to Cys62, as revealed by the assay for mixed disulfide formation with RNC 82-aa ([Figures 2D and 2E](#)). Also, the present finding that PDI and ERp46 share the binding site on the HSA nascent chain seems to explain the possible competition of PDI with ERp46 for binding the RNC ([Figures S2B and S2C](#)).

Role of the PDI hydrophobic pocket in oxidation of the HSA nascent chain

It is widely known that the PDI b' domain contains a hydrophobic pocket that acts as a primary substrate-binding site ([Klappa et al., 1998](#)). To examine the involvement of the hydrophobic pocket in PDI-catalyzed disulfide bond formation in the HSA nascent chain, we mutated I289, one of the central residues that constitute the hydrophobic pocket, to Ala, and compared the efficiency of disulfide bond introduction into RNC 82-aa between wild-type (WT) and mutant I289A proteins. In this mutant, the x-linker flanked by b' and a' domains tightly binds the hydrophobic pocket, unlike in WT, thereby preventing PDI from tightly binding an unfolded substrate ([Bekendam et al., 2016](#); [Nguyen et al., 2008](#)). ERp57, another primary member of the PDI family, has a U-shape domain arrangement similar to PDI, but does not contain the hydrophobic pocket in the b' domain. For comparison, we also monitored ERp57-catalyzed disulfide introduction into RNC 82-aa.

Despite the occlusion or lack of the substrate-binding hydrophobic pocket, both PDI I289A and ERp57 were found to introduce a disulfide bond into RNC 82-aa at a higher rate than PDI WT ([Figures 6A and 6B](#)). This result suggests that the pocket is involved in binding the HSA nascent chain, but this binding appears to rather slow down disulfide introduction into a nascent chain.

To further explore the mechanism by which PDI I289A introduced a disulfide bond at a faster rate than PDI WT, we analyzed its binding to RNC using HS-AFM. The analysis revealed that whereas nearly one-third of PDI I289A molecules formed dimers in the presence of RNC 82-aa like PDI WT ([Figure 6C](#)), the mutant dimers bound RNC for a shorter time than the WT dimers ([Figures 6D and S5B and Video S6](#)). PDI I289A monomers bound RNC for even shorter time, like WT monomers ([Figures 6D and S5A and Video S5](#)). As a result, PDI I289A showed similar RNC-binding time to ERp46 ([Figures 5D and 6D](#)), which likely explains the higher turnover rate of PDI I289A than that of PDI WT during the catalysis of nascent-chain disulfide bond formation. PDI I289A also bound RNCs at positions ~16 nm distant from ribosome with a single-Gaussian distribution ([Figure 6E](#)), suggesting that PDI I289A recognizes similar sites of the HSA nascent chain as PDI and ERp46.

DISCUSSION

A number of studies have recently investigated co-translational oxidative folding in the ER ([Kadokura et al., 2020](#); [Robinson et al., 2017, 2020](#)). The present study showed that whereas both PDI and ERp46 can introduce a disulfide bond into a nascent chain co-translationally, ERp46 catalyzes this reaction more efficiently than PDI and requires a shorter nascent chain segment exposed outside the ribosome exit. Thus, ERp46 appears to be capable of introducing a disulfide bond into a nascent chain during the earlier stages of translation than PDI. The efficient introduction of a Cys53-Cys62 native disulfide on RNC 82-aa by ERp46 ([Figure 2](#)) suggests that a separation of ~8 aa residues between a C-terminal cysteine on a nascent chain and the ribosome exit site (i.e., residues 63–70) is sufficient for ERp46 to catalyze this reaction ([Figure 7](#)). When a nascent chain was elongated by the insertion of [SG]-repeat sequences, PDI could also introduce the native disulfide bond into RNCs to some extent ([Figures 3B and 3C](#)). Thus, PDI appears to act on a nascent chain to introduce a disulfide bond when the distance between a C-terminal cysteine on a nascent chain and the ribosome exit site reaches ~18 aa residues (i.e., residues 63–70 + [SG]₅ repeat; [Figure 7](#)).

Disulfide bond formation in partially ER-exposed nascent chains was indeed observed with the ADAM10 disintegrin domain, which has a dense disulfide bonding pattern and little defined structure ([Robinson](#)

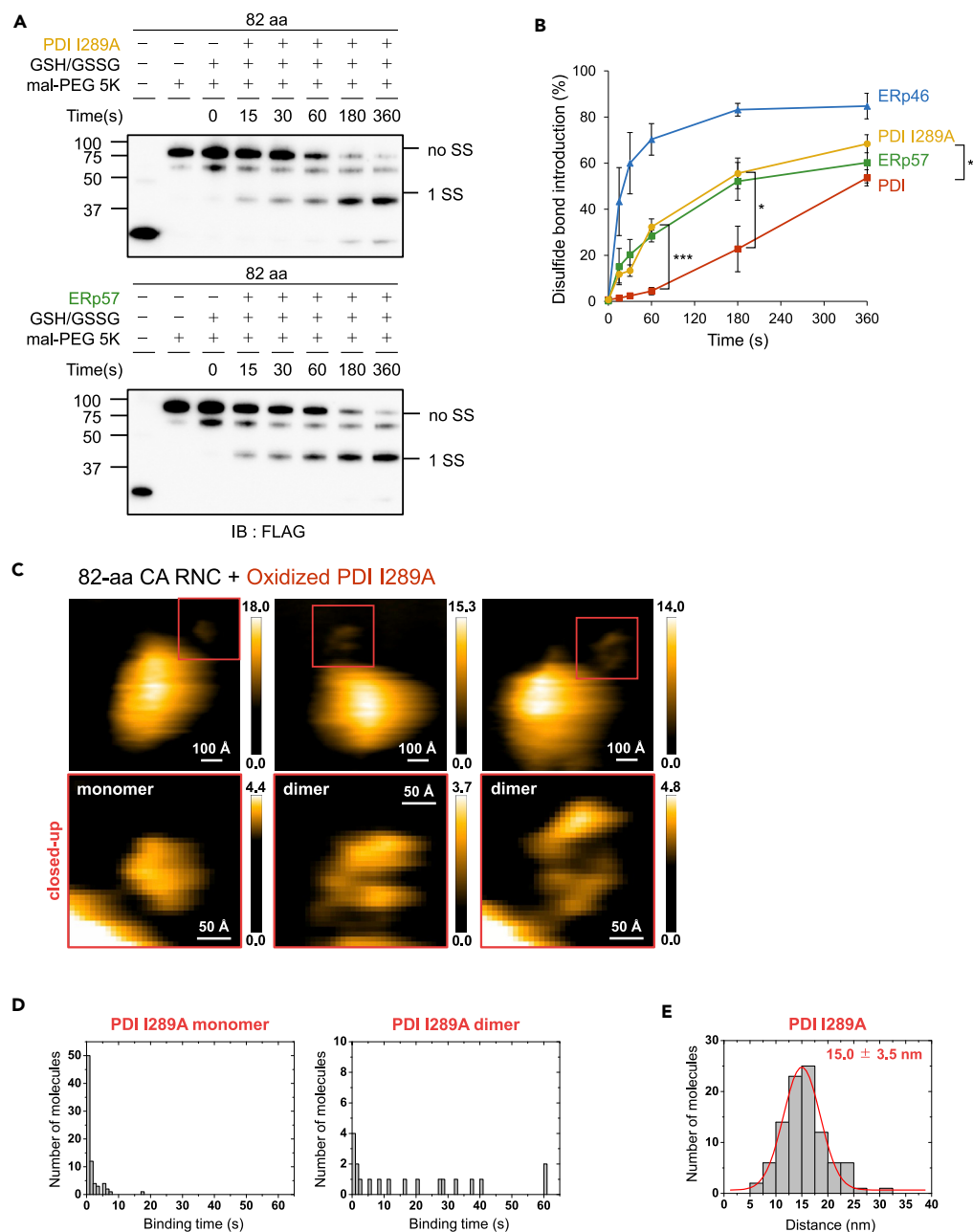


Figure 6. Role of the PDI hydrophobic pocket in PDI-mediated disulfide bond introduction into RNC 82-aa

(A) Disulfide bond introduction into RNC 82-aa by PDI I289A (upper) and ERp57 (lower). Note that faint bands observed between “no SS” and “1SS” likely represent a species in which one of cysteines is not subjected to mal-PEG modification due to glutathionylation. In support of this, these minor bands are even fainter under the conditions of no GSH/GSSG. (B) Quantification of disulfide-bonded species based on the results shown in (A). Quantifications for ERp46 and PDI are based on the results shown in Figures 1E and 1F. Statistical analysis has been made for the difference between PDI WT and PDI I289A at reaction times of 60 s, 180 s, and 360 s. * $p < 0.05$, *** $p < 0.001$. $n = 3$. Error bars indicate SD. (C) HS-AFM analyses for binding of PDI I289A to RNC 82-aa. Upper AFM images (scan area, $800 \text{ \AA} \times 800 \text{ \AA}$; scale bar, 100 \AA) display the PDI I289A molecules that bind 82-aa CA RNC, as marked by red squares. Lower images (scan area, $250 \text{ \AA} \times 250 \text{ \AA}$; scale bar, 50 \AA) highlight the regions surrounded by red squares in the upper images. (D) Histograms show the distribution of the RNC binding time of the PDI I289A monomers (left) and dimers (right). (E) Histogram shows the distribution of the distance between the edge of the ribosome and the centers of RNC-neighborhood PDI I289A molecules, calculated from the observed AFM images. Values represents the average distance (mean \pm SD) calculated from curve fitting with a single-Gaussian model.

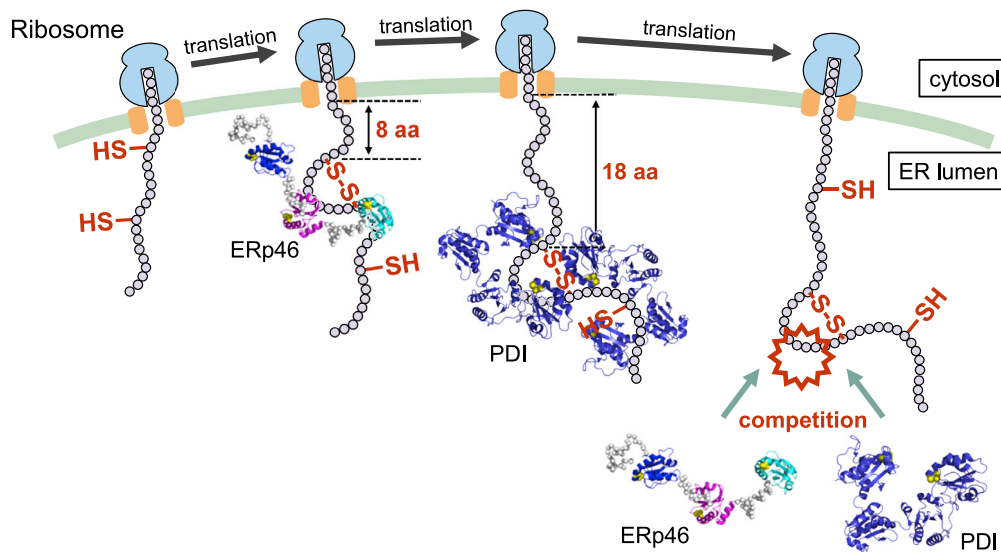


Figure 7. Proposed model of co-translational disulfide bond introduction into nascent chains by ERp46 and PDI

During the early stages of translation, ERp46 introduces disulfide bonds through transient binding to a nascent chain. For efficient disulfide introduction by ERp46, a pair of cysteines must be exposed by at least ~8 amino acids from the ribosome exit site. By contrast, PDI introduces disulfide bonds by holding a nascent chain inside the central cavity of the PDI homodimer during the later stages of translation, where a pair of cysteines must be exposed by at least ~18 amino acids from the ribosome exit site. However, when a longer polypeptide is exposed outside the ribosome, ERp46- or PDI-mediated disulfide bond formation can be slower, possibly due to formation of higher-order conformation in the nascent chain. Longer nascent chains may allow PDI family enzymes to compete with each other for binding and acting on RNC.

et al., 2020). Thus, disulfide bond formation seems to be allowed before the higher order structure is defined in a nascent chain. This could be the case with a Cys34-Cys53 nonnative disulfide and a Cys53-Cys62 native disulfide on RNC 82-aa, because the N-terminal 82-residue HSA fragment alone is unlikely to fold to a globular native-like structure, although the fragment of residue 35–56 is predicted to form an α -helix according to the HSA native structure. In contrast, some proteins including β 2-microglobulin (β 2M) and prolactin are shown to form disulfide bonds only after a folding domain is fully exposed to the ER or a polypeptide chain is released from ribosome, suggesting their folding-driven disulfide bond formation. Notably, PDI binds β 2M when the N-terminal ~80 residues of β 2M are exposed to the ER and completes disulfide bond introduction at the even later stages of translation (Robinson et al., 2017). Thus PDI has been demonstrated to engage in disulfide bond formation during late stages of translation or after translation in the ER.

Regarding mechanistic insight, the present HS-AFM analysis visualized PDI and ERp46 acting on nascent chains at the single-molecule level. We found that PDI forms a face-to-face homodimer that binds a nascent chain, as is the case with reduced and denatured full-length substrates (Okumura et al., 2019). On the other hand, ERp46 maintains a monomeric form while binding a nascent chain. Interestingly, the PDI dimer binds a nascent chain much more persistently than the PDI monomer and ERp46, suggesting that the PDI dimer holds a nascent chain tightly inside its central hydrophobic cavity. In agreement with this observation, a hydrophobic-pocket mutant (I289A) of PDI bound a nascent chain for shorter time and introduced a disulfide bond into a nascent chain more rapidly than the WT enzyme, similarly to ERp46. Also, PDI inhibited ERp46-mediated disulfide introduction probably due to its competition with ERp46 for binding the similar sites of RNC 95-aa (Figures 7, 5E and S2). Thus, PDI family enzymes do not always work synergistically to accelerate oxidative protein folding, but may possibly inhibit each other during co-translational disulfide bond formation.

How the ER membrane translocon channel is involved in co-translational oxidative folding catalyzed by PDI family enzymes remains an important question. It is possible that PDI and ERp46 form a supramolecular complex with ribosomes and the Sec61 translocon channel via a nascent chain. Indeed, PDI was previously identified as a luminal protein that was in close contact with translocating nascent chains (Klappa et al.,

1995). Additionally, the oligosaccharyltransferase complex (Harada et al., 2009) and an ER chaperone calnexin (Farmery et al., 2000) have been reported to interact with the ribosome-associated Sec61 channel to catalyze N-glycosylation and folding of nascent chains in the ER, respectively. In this regard, it will be interesting to examine the close co-localization of PDI/ERp46 with the Sec61 channel in the presence or absence of nascent chains in transit into the ER lumen by super-resolution microscopy or other tools. Systematic studies with a wider range of substrates of different lengths from the ribosome exit site and different numbers of cysteine pairs, and with other PDI family members potentially having different functional roles, will provide further mechanistic and physiological insights into co-translational oxidative folding and protein quality control in the ER.

Limitations of the study

In this study, we constructed and employed three types of HSA nascent chains RNC 69-aa, 82-aa, and 95-aa as model substrates. It will be interesting to prepare additional HSA nascent chain constructs with different lengths and different numbers of disulfide bonds and investigate their disulfide bond formation catalyzed by PDI and ERp46. We would thereby be able to discuss the detailed mechanisms of co-translational oxidative folding of HSA. We also need to note that under the physiological setting, nascent chains enter the ER through the Sec61 translocon channel. Functional significance of the interplay between the translocon channel and PDIs remains an important open question.

Resource availability

Lead contact

Further information and requests for resources and reagents should be directed to and will be fulfilled by the lead contact, Kenji Inaba (kenji.inaba.a1@tohoku.ac.jp).

Materials availability

All unique and stable reagents generated in this study are available from the lead contact with a completed Materials Transfer Agreement.

Data and code availability

This study did not generate datasets.

METHODS

All methods can be found in the accompanying [transparent methods supplemental file](#).

SUPPLEMENTAL INFORMATION

Supplemental information can be found online at <https://doi.org/10.1016/j.isci.2021.102296>.

ACKNOWLEDGMENTS

This work was supported by Grants-in-Aid for Scientific Research from MEXT to K.I. (26116005 and 18H03978), the NAGASE Science Technology Foundation (K.I.), and the MITSUBISHI Foundation (K.I.). This work was also supported by Grant-in-Aid for JSPS Fellows (Grant Number 20J11932 to C.H.) and a Grant-in-Aid of Tohoku University, Division for Interdisciplinary Advanced Research and Education (to C.H.).

AUTHOR CONTRIBUTIONS

C.H. and T.M. developed an experimental system for directly monitoring co-translational disulfide bond formation. K.M. and H.I. developed and prepared cell-free protein translation system reconstituted with human factors. C.H. prepared various plasmids. C.H. and M.O. purified PDI and ERp46, and their mutants. C.H. and K.N. performed HS-AFM measurements and analyses. C.H., K.N., M.O., and T.O. discussed the results of HS-AFM. K.I. supervised the work. C.H. and K.N. prepared the figures. C.H. and K.I. wrote the manuscript. All the authors discussed the results and approved the manuscript.

DECLARATION OF INTERESTS

We declare that there are no competing interests related to this work.

Received: September 29, 2020

Revised: January 13, 2021

Accepted: March 5, 2021

Published: April 23, 2021

REFERENCES

- Alderete, J.P., Jarrahan, S., and Geballe, A.P. (1999). Translational effects of mutations and polymorphisms in a repressive upstream open reading frame of the human cytomegalovirus UL4 gene. *J. Virol.* **73**, 8330–8337.
- Araki, K., and Inaba, K. (2012). Structure, mechanism, and evolution of Ero1 family enzymes. *Antioxid. Redox Signal.* **16**, 790–799.
- Bekendam, R.H., Bendapudi, P.K., Lin, L., Nag, P.P., Pu, J., Kennedy, D.R., Feldenzer, A., Chiu, J., Cook, K.M., Furie, B., et al. (2016). A substrate-driven allosteric switch that enhances PDI catalytic activity. *Nat. Commun.* **7**, 12579.
- Buhr, F., Jha, S., Thommen, M., Mittelstaet, J., Kutz, F., Schwalbe, H., Rodnina, M.V., and Komar, A.A. (2016). Synonymous codons direct cotranslational folding toward different protein conformations. *Mol. Cell* **61**, 341–351.
- Bulleid, N.J., and Ellgaard, L. (2011). Multiple ways to make disulfides. *Trends Biochem. Sci.* **36**, 485–492.
- Chadani, Y., Niwa, T., Izumi, T., Sugata, N., Nagao, A., Suzuki, T., Chiba, S., Ito, K., and Taguchi, H. (2017). Intrinsic ribosome destabilization underlies translation and provides an organism with a strategy of environmental sensing. *Mol. Cell* **68**, 528–539.e525.
- Farmery, M.R., Allen, S., Allen, A.J., and Bulleid, N.J. (2000). The role of ERp57 in disulfide bond formation during the assembly of major histocompatibility complex class I in a synchronized semipermeabilized cell translation system. *J. Biol. Chem.* **275**, 14933–14938.
- Harada, Y., Li, H., Li, H., and Lennarz, W.J. (2009). Oligosaccharyltransferase directly binds to ribosome at a location near the translocon-binding site. *Proc. Natl. Acad. Sci. U S A* **106**, 6945–6949.
- Hartl, F.U., Bracher, A., and Hayer-Hartl, M. (2011). Molecular chaperones in protein folding and proteostasis. *Nature* **475**, 324–332.
- Kadokura, H., Dazai, Y., Fukuda, Y., Hirai, N., Nakamura, O., and Inaba, K. (2020). Observing the nonvectorial yet cotranslational folding of a multidomain protein, LDL receptor, in the ER of mammalian cells. *Proc. Natl. Acad. Sci. U S A* **117**, 16401–16408.
- Klappa, P., Freedman, R.B., and Zimmermann, R. (1995). Protein disulfide isomerase and a luminal cyclophilin-type peptidyl prolyl cis-trans isomerase are in transient contact with secretory proteins during late stages of translocation. *Eur. J. Biochem.* **232**, 755–764.
- Klappa, P., Ruddock, L.W., Darby, N.J., and Freedman, R.B. (1998). The b' domain provides the principal peptide-binding site of protein disulfide isomerase but all domains contribute to binding of misfolded proteins. *EMBO J.* **17**, 927–935.
- Kodera, N., Yamamoto, D., Ishikawa, R., and Ando, T. (2010). Video imaging of walking myosin V by high-speed atomic force microscopy. *Nature* **468**, 72–76.
- Kojima, R., Okumura, M., Masui, S., Kanemura, S., Inoue, M., Saiki, M., Yamaguchi, H., Hikima, T., Suzuki, M., Akiyama, S., et al. (2014). Radically different thioredoxin domain arrangement of ERp46, an efficient disulfide bond introducer of the mammalian PDI family22 (Structure), pp. 431–443.
- Koritzinsky, M., Levitin, F., van den Beucken, T., Rumentir, R.A., Harding, N.J., Chu, K.C., Boutros, P.C., Braakman, I., and Wouters, B.G. (2013). Two phases of disulfide bond formation have differing requirements for oxygen. *J. Cell Biol.* **203**, 615–627.
- Lee, J.Y., and Hirose, M. (1992). Partially folded state of the disulfide-reduced form of human serum albumin as an intermediate for reversible denaturation. *J. Biol. Chem.* **267**, 14753–14758.
- Machida, K., Mikami, S., Masutani, M., Mishima, K., Kobayashi, T., and Imataka, H. (2014). A translation system reconstituted with human factors proves that processing of encephalomyocarditis virus proteins 2A and 2B occurs in the elongation phase of translation without eukaryotic release factors. *J. Biol. Chem.* **289**, 31960–31971.
- Matsuo, Y., Ikeuchi, K., Saeki, Y., Iwasaki, S., Schmidt, C., Udagawa, T., Sato, F., Tsuchiya, H., Becker, T., Tanaka, K., et al. (2017). Ubiquitination of stalled ribosome triggers ribosome-associated quality control. *Nat. Commun.* **8**, 159.
- Mezghrani, A., Fassio, A., Benham, A., Simmen, T., Braakman, I., and Sitia, R. (2001). Manipulation of oxidative protein folding and PDI redox state in mammalian cells. *EMBO J.* **20**, 6288–6296.
- Molinari, M., and Helenius, A. (1999). Glycoproteins form mixed disulphides with oxidoreductases during folding in living cells. *Nature* **402**, 90–93.
- Nguyen, V.D., Saaranen, M.J., Karala, A.R., Lappi, A.K., Wang, L., Raykhel, I.B., Alanen, H.I., Salo, K.E., Wang, C.C., and Ruddock, L.W. (2011). Two endoplasmic reticulum PDI peroxidases increase the efficiency of the use of peroxide during disulfide bond formation. *J. Mol. Biol.* **406**, 503–515.
- Nguyen, V.D., Wallis, K., Howard, M.J., Haapalainen, A.M., Salo, K.E., Saaranen, M.J., Sidhu, A., Wierenga, R.K., Freedman, R.B., Ruddock, L.W., et al. (2008). Alternative conformations of the x region of human protein disulfide-isomerase modulate exposure of the substrate binding b' domain. *J. Mol. Biol.* **383**, 1144–1155.
- Noi, K., Yamamoto, D., Nishikori, S., Arita-Morioka, K., Kato, T., Ando, T., and Ogura, T. (2013). High-speed atomic force microscopic observation of ATP-dependent rotation of the AAA+ chaperone p9721 (Structure), pp. 1992–2002.
- Okumura, M., Kadokura, H., and Inaba, K. (2015). Structures and functions of protein disulfide isomerase family members involved in proteostasis in the endoplasmic reticulum. *Free Radic. Biol. Med.* **83**, 314–322.
- Okumura, M., Noi, K., Kanemura, S., Kinoshita, M., Saio, T., Inoue, Y., Hikima, T., Akiyama, S., Ogura, T., and Inaba, K. (2019). Dynamic assembly of protein disulfide isomerase in catalysis of oxidative folding. *Nat. Chem. Biol.* **15**, 499–509.
- Robinson, P.J., and Bulleid, N.J. (2020). Mechanisms of disulfide bond formation in nascent polypeptides entering the secretory pathway. *Cells* **9**, 1994.
- Robinson, P.J., Kanemura, S., Cao, X., and Bulleid, N.J. (2020). Protein secondary structure determines the temporal relationship between folding and disulfide formation. *J. Biol. Chem.* **295**, 2438–2448.
- Robinson, P.J., Pringle, M.A., Woolhead, C.A., and Bulleid, N.J. (2017). Folding of a single domain protein entering the endoplasmic reticulum precedes disulfide formation. *J. Biol. Chem.* **292**, 6978–6986.
- Rutkevich, L.A., Cohen-Doyle, M.F., Brockmeier, U., and Williams, D.B. (2010). Functional relationship between protein disulfide isomerase family members during the oxidative folding of human secretory proteins. *Mol. Biol. Cell* **21**, 3093–3105.
- Rutkevich, L.A., and Williams, D.B. (2012). Vitamin K epoxide reductase contributes to protein disulfide formation and redox homeostasis within the endoplasmic reticulum. *Mol. Biol. Cell* **23**, 2017–2027.
- Sato, Y., and Inaba, K. (2012). Disulfide bond formation network in the three biological kingdoms, bacteria, fungi and mammals. *FEBS J.* **279**, 2262–2271.
- Sato, Y., Kojima, R., Okumura, M., Hagiwara, M., Masui, S., Maegawa, K., Saiki, M., Horibe, T., Suzuki, M., and Inaba, K. (2013). Synergistic cooperation of PDI family members in peroxiredoxin 4-driven oxidative protein folding. *Sci. Rep.* **3**, 2456.
- Schulman, S., Wang, B., Li, W., and Rapoport, T.A. (2010). Vitamin K epoxide reductase prefers ER membrane-anchored thioredoxin-like redox partners. *Proc. Natl. Acad. Sci. U S A* **107**, 15027–15032.
- Sugio, S., Kashima, A., Mochizuki, S., Noda, M., and Kobayashi, K. (1999). Crystal structure of human serum albumin at 2.5 Å resolution. *Protein Eng.* **12**, 439–446.

Tavender, T.J., and Bulleid, N.J. (2010). Molecular mechanisms regulating oxidative activity of the Ero1 family in the endoplasmic reticulum. *Antioxid. Redox Signal.* 13, 1177–1187.

Tavender, T.J., Springate, J.J., and Bulleid, N.J. (2010). Recycling of peroxiredoxin IV provides a novel pathway for disulphide formation in the endoplasmic reticulum. *EMBO J.* 29, 4185–4197.

Tian, G., Xiang, S., Noiva, R., Lennarz, W.J., and Schindelin, H. (2006). The crystal structure of yeast protein disulfide isomerase suggests cooperativity between its active sites. *Cell* 124, 61–73.

Uchihashi, T., Watanabe, Y.H., Nakazaki, Y., Yamasaki, T., Watanabe, H., Maruno, T., Ishii, K., Uchiyama, S., Song, C., Murata, K., et al. (2018). Dynamic structural states of ClpB involved in its disaggregation function. *Nat. Commun.* 9, 2147.

Wang, C., Yu, J., Huo, L., Wang, L., Feng, W., and Wang, C.C. (2012). Human protein-disulfide isomerase is a redox-regulated chaperone activated by oxidation of domain a'. *J. Biol. Chem.* 287, 1139–1149.

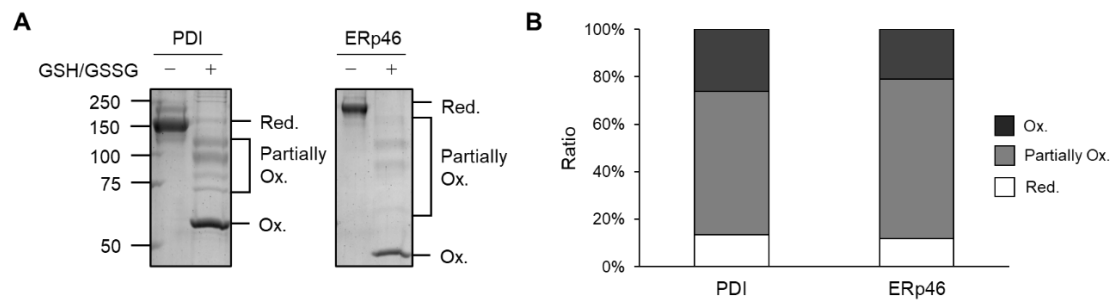
Zhang, Y., Wölfe, T., and Rospert, S. (2013). Interaction of nascent chains with the ribosomal tunnel proteins Rpl4, Rpl17, and Rpl39 of *Saccharomyces cerevisiae*. *J. Biol. Chem.* 288, 33697–33707.

iScience, Volume 24

Supplemental information

Distinct roles and actions of protein disulfide isomerase family enzymes in catalysis of nascent-chain disulfide bond formation

Chihiro Hirayama, Kodai Machida, Kentaro Noi, Tadayoshi Murakawa, Masaki Okumura, Teru Ogura, Hiroaki Imataka, and Kenji Inaba

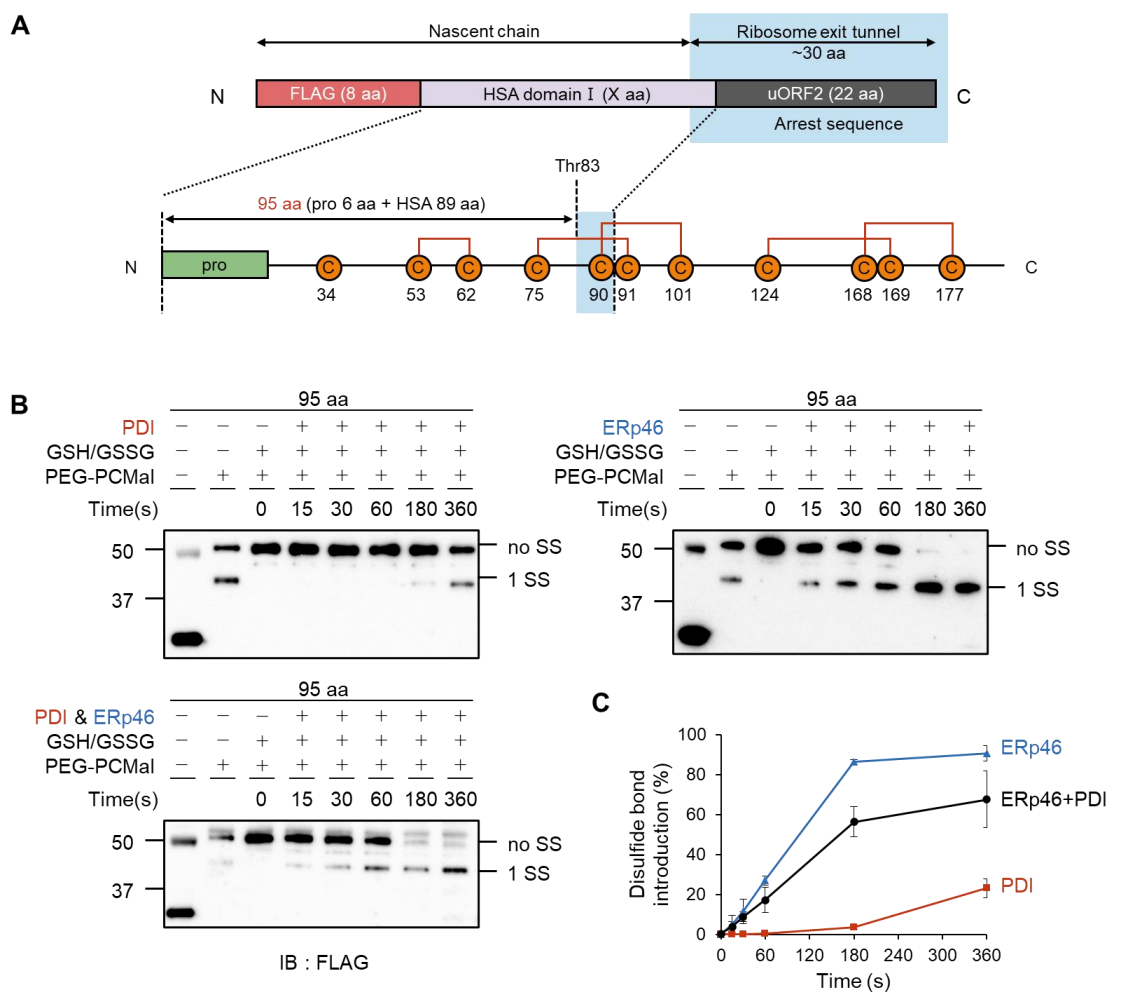


1

2 **Figure S1. Redox states of PDI and ERp46 in glutathione redox buffer, Related to**
 3 **Figure 1.**

4 (A) Redox states of PDI and ERp46 in the presence of 1 mM GSH and 0.2 mM GSSG.
 5 Purified PDI and ERp46 were incubated for 6 mins at 30 °C in the above glutathione
 6 redox buffer and modified with 2 mM mal-PEG 5K for separation on SDS gels.

7 (B) Quantification based on the results shown in (A).



8

9 **Figure S2. Disulfide bond introduction into RNC 95-aa by PDI and ERp46, Related**
 10 **to Figure 1**

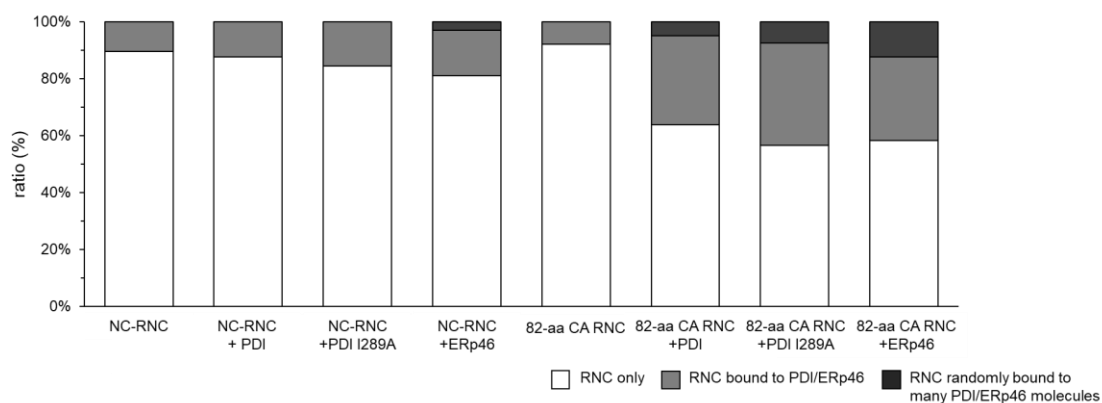
11 (A) Schematic structure of RNC-95-aa. Orange circles and red lines in the bottom cartoon
 12 indicate cysteines and native disulfides, respectively. The region predicted to be buried in
 13 the ribosome exit tunnel is shown by a cyan box.

14 (B) Time course of PDI (0.1 μ M)-, ERp46 (0.1 μ M)-, and their mixture (0.1 μ M each)-
 15 catalyzed disulfide bond introduction into RNC 95-aa. 'noSS' and '1SS' denote reduced
 16 and single-disulfide-bonded species of the HSA nascent chain, respectively.

17 (C) Quantification of the single-disulfide-bonded (1 SS) species based on the result shown
 18 in (B) (n = 3).

A

	RNC only	RNC bound to PDI/ERp46	RNC bound to many PDI/ERp46 molecules	total
NC-RNC	94	11	0	105
NC-RNC + PDI	106	15	0	121
NC-RNC + PDI I289A	87	16	0	103
NC-RNC + ERp46	81	16	3	100
82-aa CA RNC	116	10	0	126
82-aa RNC CA + PDI	141	69	11	221
82-aa RNC CA + PDI I289A	115	73	15	203
82-aa RNC CA + ERp46	117	59	25	201

B

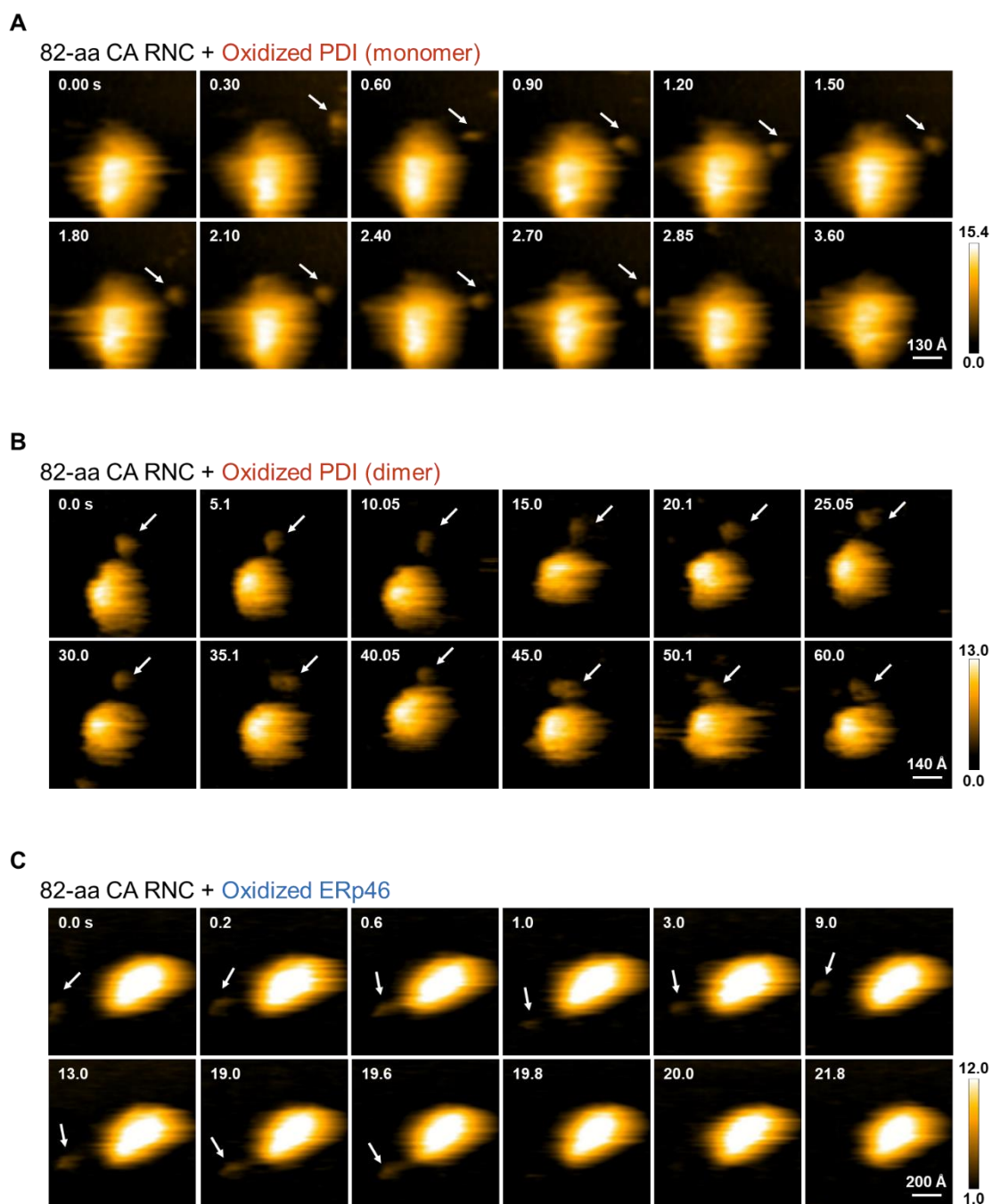
20

21 **Figure S3. Statistical analysis of RNC molecules observed by HS-AFM in the**
 22 **presence or absence of PDI/ERp46, Related to Figures 5 and 6.**

23 (A) Number of particles observed for NC-RNC or 82-aa CA RNC molecules present in
 24 isolation or bound to PDI/ERp46 molecules.

25 (B) Ratio of NC-RNC or 82-aa CA RNC molecules present in isolation or bound to
 26 PDI/ERp46, calculated based on the observed number of particles in (A). Note that a
 27 minor portion of NC-RNC or 82-aa CA RNC molecules were bound to many ERp46/PDI
 28 molecules, possibly due to serious structural damages of the RNC molecules.

29



30

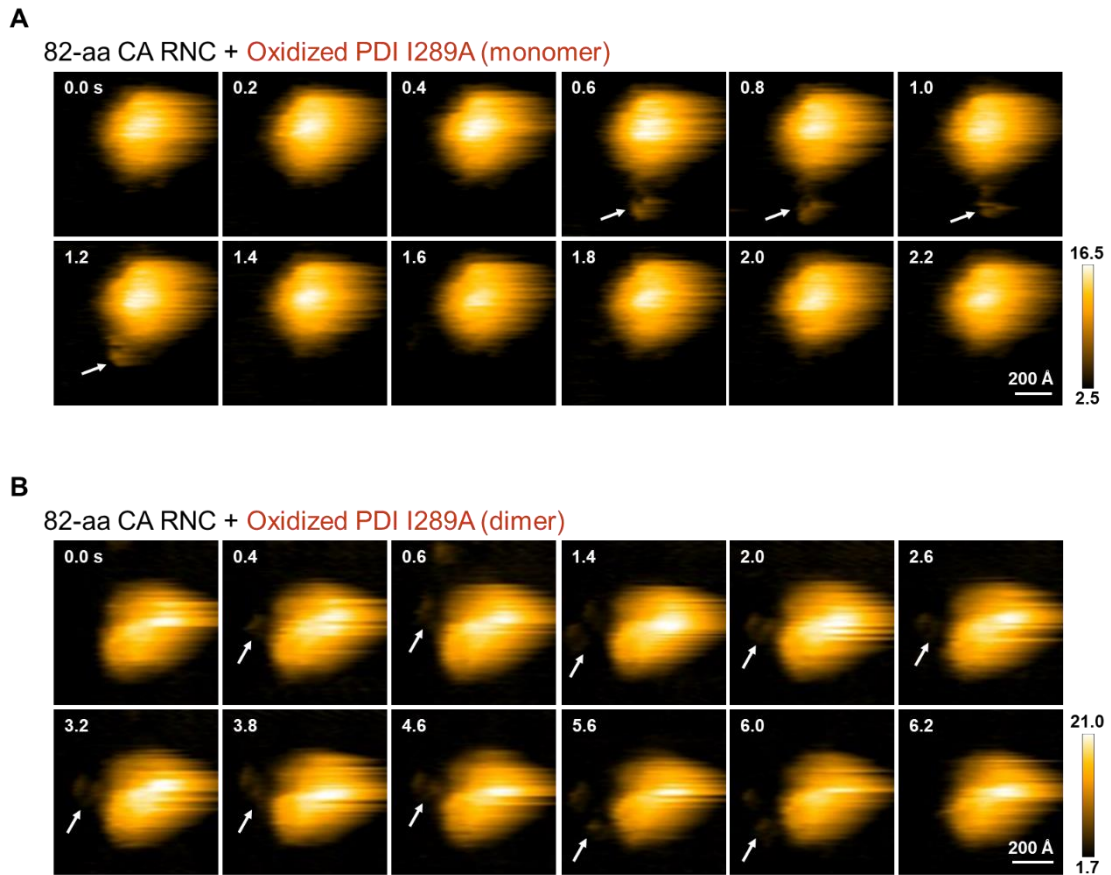
31 **Figure S4. Representative time-course snapshots captured by HS-AFM for 82-aa CA**
 32 **RNC bound to the PDI monomer (A), the PDI dimer (B), and ERp46 (C), Related to**
 33 **Figure 5**

34 (A) Time-course snapshots captured by HS-AFM for the PDI monomer binding to 82-aa
 35 CA RNC. The AFM images (scan area, $650 \text{ \AA} \times 650 \text{ \AA}$; scale bar, 130 \AA) displaying 82-
 36 aa CA RNC in the presence of oxidized PDI (1 nM). White arrows indicate the monomeric

37 PDI molecules that bind to 82-aa CA RNC. See also supplementary video 2.

38 (B) Time-course snapshots captured by HS-AFM for the PDI dimer binding to 82-aa CA
39 RNC. The AFM images (scan area, $700 \text{ \AA} \times 700 \text{ \AA}$; scale bar, 140 \AA) displaying 82-aa
40 CA RNC in the presence of oxidized PDI (1 nM). White arrows indicate the dimeric PDI
41 molecules that bind to 82-aa CA RNC. See also supplementary video 3.

42 (C) Time-course snapshots captured by HS-AFM for ERp46 binding to 82-aa CA RNC.
43 The AFM images (scan area, $1,000 \text{ \AA} \times 1,000 \text{ \AA}$; scale bar, 200 \AA) displaying 82-aa CA
44 RNC in the presence of oxidized ERp46 (1 nM). White arrows indicate the ERp46
45 molecules that bind to 82-aa CA RNC. See also supplementary video 4.



46

47 **Figure S5. Representative time-course snapshots captured by HS-AFM for 82-aa CA**
 48 **RNC bound to the PDI I289A monomer (A), and the PDI I289A dimer (B), Related**
 49 **to Figure 6**

50 (A) Time-course snapshots captured by HS-AFM for the PDI I289A monomer binding to
 51 82-aa CA RNC. The AFM images (scan area, $900 \text{ \AA} \times 900 \text{ \AA}$; scale bar, 200 \AA) displaying
 52 82-aa CA RNC in the presence of oxidized PDI I289A (1 nM). White arrows indicate the
 53 monomeric PDI I289A molecules that bind to 82-aa CA RNC. See also supplementary
 54 video 5.

55 (B) Time-course snapshots captured by HS-AFM for the PDI I289A dimer binding to 82-
 56 aa CA RNC. The AFM images (scan area, $800 \text{ \AA} \times 800 \text{ \AA}$; scale bar, 200 \AA) displaying
 57 82-aa CA RNC in the presence of oxidized PDI I289A (1 nM). White arrows indicate the
 58 dimeric PDI I289A molecules that bind to 82-aa CA RNC. See also supplementary
 59 video 6.

60 **Supplemental table**61 **Table S1 – Primers used in this study, Related to Figures 2 and 3**

No.	Plasmid name	template	Mutation position	Primer name	Nucleic acid sequence (5'-3')
1	82 aa C34A	82 aa	C34A	HSA C34A FW	cag tat ctt cag cag gcc cca ttt gaa gat cat
				HSA C34A RV	atg atc ttc aaa tgg ggc ctg ctg aag ata ctg
2	82 aa C53A	82 aa	C53A	HSA C53A FW	gaa ttt gca aaa aca gcc gtt gct gat gag tca
				HSA C53A RV	tga ctc atc agc aac ggc tgt ttt tgc aaa ttc
3	82 aa C62A	82 aa	C62A	HSA C62A FW	gag tca gct gaa aat gcc gac aaa tca ctt cat
				HSA C62A RV	atg aag tga ttt gtc ggc att ttc agc tga ctc
4	82 aa mono-Cys34	82 aa C53A	C62A	HSA C62A FW	gag tca gct gaa aat gcc gac aaa tca ctt cat
				HSA C62A RV	atg aag tga ttt gtc ggc att ttc agc tga ctc
5	82 aa mono-Cys53	82 aa C34A	C62A	HSA C62A FW	gag tca gct gaa aat gcc gac aaa tca ctt cat
				HSA C62A RV	atg aag tga ttt gtc ggc att ttc agc tga ctc
6	82 aa mono-Cys62	82 aa C34A	C53A	HSA C53A FW	gaa ttt gca aaa aca gcc gtt gct gat gag tca
				HSA C53A RV	tga ctc atc agc aac ggc tgt ttt tgc aaa ttc
7	82 aa C34A [SG] ₅	82 aa C34A	between L74 and C75	C34A 5rpt 10rpt FW2	ggc agc ggc agc ggc tgc aca gaa ttc atg cag
				C34A SG5rpt RV	gcc gct gcc gct gcc gct gcc gct gcc gct taa ttt gtc tcc aaa aag
8	82 aa C34A [SG] ₁₀	82 aa C34A	between L74 and C75	C34A 5rpt 10rpt FW2	ggc agc ggc agc ggc tgc aca gaa ttc atg cag
				C34A SG10rpt RV	gcc gct gcc gct gcc gct gcc gct gcc gct gcc gct gcc gct gcc gct taa ttt gtc tcc aaa aag

62

63

64

65 **Transparent Methods**

66 **Construction of HSA plasmids**

67 DNA fragments encoding specific regions (69-aa, N-terminal pro-sequence 6-aa + the
68 subsequent 63-aa; 82-aa, N-terminal pro-sequence 6-aa + the subsequent 76-aa; 95-aa, N-
69 terminal pro-sequence 6-aa + the subsequent 89-aa) of HSA were amplified by PCR with
70 appropriate primers and inserted into the pUC-T7-HCV-FLAG-2A-uORF expression
71 plasmid, as described in Machida et al. (2014). The amplified fragments were replaced
72 with the 2A region to generate pUC-T7-HCV-FLAG-HSA (69-aa or 82-aa)-uORF2. RNC
73 82-aa C34A/C53A/C62A and mono-Cys mutants were constructed using the QuikChange
74 method with appropriate primers (Table S1). RNC 82-aa C34A with [SG]₅ or [SG]₁₀
75 repeats were constructed by the Prime STAR MAX (Takara Bio Inc., Japan) method using
76 appropriate primers (Table S1).

77

78 **Expression and purification of PDI and ERp46**

79 Overexpression and purification of human PDI and ERp46, and their mutants, were
80 performed as described previously (Kojima et al., 2014; Sato et al., 2013). An ERp46
81 trapping mutant with a CXXA sequence in all Trx-like domains was constructed by the
82 QuikChange method using appropriate sets of primers.

83

84 **Preparation of RNCs using a translation system reconstituted with human factors**

85 A cell-free translation system was reconstituted with eEF1 (50 μ M), eEF2 (1 μ M), eRF1/3
86 (0.5 μ M), aminoacyl-tRNA synthetases (0.15 μ g/ μ l), tRNAs (1 μ g/ μ l), 40S ribosomal
87 subunit (0.5 μ M), 60S ribosomal subunit (0.5 μ M), PPA1 (0.0125 μ M), amino acids

88 mixture (0.1 mM) and T7 RNA polymerase (0.015 $\mu\text{g}/\mu\text{l}$) (Machida et al., 2014). We
89 added 1.0 μL template plasmid (0.5 mg/mL) into 19 μL of this cell-free system, and the
90 mixture was incubated for at least 3–4.5 h at 32°C. After HKMS buffer (comprising 25
91 mM HEPES-KOH (pH 7.0), 150 mM KCl, 5 mM $\text{Mg}(\text{OAc})_2$, and 1.0 M sucrose) was
92 added, samples were ultra-centrifuged at 100,000 g overnight at 4 °C to recover the RNC
93 as a pellet. After removing the supernatant, pellets were resuspended in HKM buffer
94 comprising 25 mM HEPES-KOH (pH 7.0), 150 mM KCl, and 5 mM $\text{Mg}(\text{OAc})_2$.

95

96 **Monitoring PDI- and ERp46-mediated disulfide bond introduction into RNCs**

97 The RNC suspension prepared as described above was mixed with PDI or ERp46 (0.1
98 μM each) and glutathione/oxidized glutathione (GSH/GSSG; 1.0 mM:0.2 mM;
99 NACALAI TESQUE, INC., Japan). Aliquots were collected after incubation at 30°C for
100 the indicated times, and reactions were quenched with mal-PEG 5K (2 mM; NOF
101 CORPORATION, Japan) for RNC 69-aa and RNC 82-aa. After cysteine alkylation at
102 room temperature for 20 min, samples were separated by 12% Bis-Tris (pH7.0) PAGE
103 (Thermo Fisher Scientific K.K., Japan) in the presence of the reducing reagent β -
104 mercaptoethanol (β -ME; 10% v/v; NACALAI TESQUE, INC., Japan). After transferring
105 onto a polyvinylidene fluoride (PVDF) membrane (Merck KGaA, Darmstadt, Germany),
106 bands on the membrane were visualized using Chemi-Lumi One Ultra (NACALAI
107 TESQUE, INC., Japan) and a ChemiDoc™ Imaging System (Bio-Rad Laboratories, Inc.,
108 CA, USA). Signal intensity was quantified using ImageLab software (Bio-Rad
109 Laboratories, Inc., CA, USA).

110 For RNC 95-aa, reactions were quenched with PEG-PCMal (Dojindo, Japan).

111 After cysteine alkylation at room temperature for 20 min, samples were separated by 10%
112 Bis-Tris (pH7.0) PAGE (Thermo Fisher Scientific K.K., Japan) in the presence of the
113 reducing reagent β -ME (10% v/v;). After gel electrophoresis, the gel was subjected to UV
114 irradiation (302 nm, 8 W) for 30 min. The subsequent procedures were the same as
115 described above.

116

117 **Monitoring intermolecular disulfide bond linkage between PDI/ERp46 and** 118 **ribosome-HSA nascent chain complexes**

119 To detect the intermolecular disulfide bond linkage between PDI/ERp46 and the
120 ribosome-HSA nascent chain complex, we employed RNC 82-aa mono-Cys mutants
121 retaining one of Cys34, Cys53, or Cys62. The RNC suspension prepared as described
122 above was mixed with a PDI or ERp46 trapping mutant (1 μ M each) and diamide (100
123 μ M). Aliquots were collected after incubation at 30°C for 10 min, and reactions were
124 quenched with N-ethylmaleimide (2 mM; NACALAI TESQUE, INC., Japan). Samples
125 were analyzed by Nu-PAGE and western blotting as described above.

126

127 **High-speed atomic force microscopy imaging**

128 The structural dynamics of PDI and ERp46 were probed using a high-speed AFM
129 instrument developed by Toshio Ando's group (Kanazawa University). Data acquisition
130 for ERp46 was performed as described previously (Okumura et al., 2019). Briefly, His₆-
131 tagged ERp46 was immobilized on a Co²⁺-coated mica surface through the N-terminal
132 His-tag. To this end, a droplet (10 μ L) containing 1 nM ERp46 was loaded onto the mica
133 surface. After a 3 min incubation, the surface was washed with TRIS buffer (50 mM
134 TRIS-HCl pH7.4, 300 mM NaCl). Single-molecule imaging was performed in tapping

135 mode (spring constant, ~ 0.1 N/m; resonant frequency, 0.8–1 MHz; quality factor in water,
136 ~ 2) and analyzed using Kodec4.4.7.39 software developed by Toshio Ando's group
137 (Kanazawa University). AFM observations were made in fixed imaging areas (400×400
138 \AA^2) at a scan rate of 0.1 s/frame. Each molecule was observed separately on a single frame
139 with the highest pixel setting (60×60 pixels). Cantilevers (Olympus, Tokyo, Japan) were
140 $6\text{--}7$ μm long, 2 μm wide, and 90 nm thick. For AFM imaging, the free oscillation
141 amplitude was set to ~ 1 nm, and the set-point amplitude was around 80% of the free
142 oscillation amplitude. The estimated tapping force was <30 pN. A low-pass filter was
143 used to remove noise from acquired images. The area of a single ERp46 molecule in each
144 frame was calculated using LabView 2013 (National Instruments, Austin, TX, USA) with
145 custom-made programs.

146 To observe the binding of PDI/ERp46 to RNCs by HS-AFM, RNCs were
147 immobilized on a Ni^{2+} -coated mica surface via electrostatic interactions. To this end, a
148 droplet (10 μL) containing RNCs was loaded onto the mica surface. After a 10 min
149 incubation, the surface was washed with HSA buffer comprising 25 mM HEPES-KOH
150 pH 7.0 , 150 mM KCl, and 5 mM $\text{Mg}(\text{OAc})_2$. PDI/ERp46 lacking the N-terminal His₆-tag
151 was added to the RNC-immobilized mica surface at a final concentration of 1 nM.
152 Measurements were performed under the same conditions described above.

153

154 **Supplemental References**

155 Kojima, R., Okumura, M., Masui, S., Kanemura, S., Inoue, M., Saiki, M., Yamaguchi, H.,
156 Hikima, T., Suzuki, M., Akiyama, S., *et al.* (2014). Radically different thioredoxin
157 domain arrangement of ERp46, an efficient disulfide bond introducer of the mammalian
158 PDI family. *Structure (London, England : 1993)* 22, 431-443.

159

160 Machida, K., Mikami, S., Masutani, M., Mishima, K., Kobayashi, T., and Imataka, H.
161 (2014). A translation system reconstituted with human factors proves that processing of
162 encephalomyocarditis virus proteins 2A and 2B occurs in the elongation phase of
163 translation without eukaryotic release factors. *The Journal of biological chemistry* 289,
164 31960-31971.

165

166 Okumura, M., Noi, K., Kanemura, S., Kinoshita, M., Saio, T., Inoue, Y., Hikima, T.,
167 Akiyama, S., Ogura, T., and Inaba, K. (2019). Dynamic assembly of protein disulfide
168 isomerase in catalysis of oxidative folding. *Nature chemical biology* 15, 499-509.

169

170 Sato, Y., Kojima, R., Okumura, M., Hagiwara, M., Masui, S., Maegawa, K., Saiki, M.,
171 Horibe, T., Suzuki, M., and Inaba, K. (2013). Synergistic cooperation of PDI family
172 members in peroxiredoxin 4-driven oxidative protein folding. *Scientific reports* 3, 2456.

173